Tampere University

KYRIACOS CHRYSANTHOS YIANNACOU

TWO DIMENSIONAL ACOUSTOFLUIDIC MANIPULATION OF MICROPARTICLES

Master of Science Thesis

Examiner: Prof. Pasi Kallio, Asst.Prof. Veikko Sariola

Examiner and topic approved on :

ABSTRACT

FIRSTNAME LASTNAME: KYRIACOS CHRYSANTHOS YIANNACOU
Tampere University
Master of Science Thesis,39 pages, 3 Appendix pages
March 2019
Master's Degree Programme in Automation Science and Engineering
Major: Intelligent Microsystems
Examiner: Professor Pasi Kallio, Assistant Professor Veikko Sariola
Keywords: Acoustofluidics, Micromanipulation, PMMA, Acoustofluidic device, Particle manipulation, COMSOL simulations.

Acoustically actuated microfluidic devices for bio diagnostics have gained the attention of the research community, due to the gentle and non-contact characteristics of the actuation force. The existing acoustofluidic devices have been primarily made off materials with high acoustic impedance such as glass ($Z_{\mathrm{ac}} \cong 12$ MRayls), and silicon ($Z_{\mathrm{ac}} \cong 19$ MRayls). In terms of fabrication costs and fabrication time, plastics would have been more preferable due to their rapid and easy fabrication methods such as milling, and molding into microfluidic chips. However, the drawback of using plastics in acoustofluidics is that plastics tend to have lower acoustic impedance than glass, or silicon, and are considered as lower quality resonators than e.g. glass. Nonetheless, poly-methyl methacrylate (PMMA) has a moderate acoustic impedance ($Z_{\mathrm{ac}} \cong 3$ MRayls), which is higher than e.g. PDMS where its acoustic impedance is ($Z_{\mathrm{ac}} \cong 1.03$ MRayls), and that has encouraged this work. In this thesis, the employment of bulk acoustic waves (BAW) on a two-dimensional acoustofluidic resonators made from glass and PMMA were compared for acoustofluidic micromanipulation applications. Polystyrene microparticles were used in the manipulation experiments for visualizing the acoustic modes of the acoustofluidic chips, where their frequency responses were recorded by the magnitude of motion achieved from particle tracking velocimetry (PTV). Firstly, a PMMA microfluidic device was fabricated by laser engraving, and ethanol thermal bonding. As a control experiment, a glass acoustofluidic chip was fabricated using femtosecond ablation (at Technical University of Braunschweig) and tested using the same parameters as the PMMA chip. Secondly, simulations using COMSOL Multiphysics have been carried out to determine numerical values of resonance frequencies of the devices, and their corresponding acoustic resonance mode shapes. In addition to glass and PMMA, simulations were conducted for an acoustofluidic device made out of PDMS. The simulation results showed that PDMS performance is poor for particle manipulation. Thirdly, preliminary experiments were contacted, where a beta version of our particle tracking velocimetry (PTV) was used and, we were able to obtain a rough frequency profile of the devices in the frequency range 60 kHz and 460 kHz. The results of the preliminary frequency response of the PMMA chip showed good agreement with the predicted frequency response using multiphysics simulations ,where its performance in both cases (simulations and experiments) was comparable to results obtained by the glass chip. Simulated results shown that PMMA has the potential to performs similar to the glass chip. However, in the preliminary experiments was observed that the power requirements needed for a particle motion of 0.5 mm in PMMA are much greater than in glass. This has caused overheating of the aqueous solution at antiresonances, due to the enormous amount of power fed to the actuator, which this did not happen in the glass chip. Additionally, the actual acoustic modes of both glass and PMMA chips do not agree with the simulated results, where the frequency difference in actual modes from theoretical is ~100 kHz for the glass chip.

PREFACE

This thesis is submitted as the fulfillment of the prerequisites for obtaining the degree in Master of Science in Engineering at the Tampere University (TAU). The thesis work is carried out at the Faculty of Medicine and Health Technology (MED). The following text introduces the study of acoustically manipulated particles within a microfluidic device. The study is divided into the next five chapters which are an introduction, theoretical background, methods and materials, simulations and results and conclusions.

Acknowledgments: I would like to personally thank the Academy of Finland for funding the Acoustodroplets project and also my supervisor Assistant. Professor Veikko Sariola for his excellent guidance and support during this thesis. Secondly, I would like to express my thankfulness to the Research assistant Mattern Kai, and the Professor Andreas Dietzel of the Technical University of Braunschweig for collaborating with our group, and microfabricating the glass microchip for us. Lastly, I would also like to thank all the members of my family for their constant support and encouragement.

Tampere, 2019

CONTENTS

LIST OF SYMBOLS AND ABBREVIATIONS

Symbols

A	amplitude [unitless]
c	speed of sound [m s^{-1}]
f	frequency [Hz]
E	acoustic energy density [J m^{-3}]
F_P	primary acoustic radiation force [N]
F_S	secondary acoustic radiation force[N]
k	wavenumber [rad m^{-1}]
P	pressure [Pa]
$\langle P(x) \rangle$	average pressure field [Pa]
U_{p-p}	Voltage Peak to Peak [V]
$\langle V(x) \rangle$	average velocity field [ms^{-1}]
Z	acoustic impedance [Rayls]

α	particle radius [m]
β	isentropic compressibility [Pa^{-1}]
δ	boundary vortices width [m]
Δf	frequency difference [Hz]
θ	angle [rad]
λ	wavelength [m]
ν	kinematic viscosity [$m^2 s^{-1}$]
ρ	density [kg m^{-3}]
Φ	acoustic contrast factor [unitless]
ω	angular velocity [rad s^{-1}]

Abbreviations

BAW	bulk acoustic waves
CNC	computer numerical control
LOC	lab on a chip
PDMS	polydimethylsiloxane
PMMA	poly(methyl methacrylate)
PTV	particle tracking velocimetry
PIV	particle image velocimetry
PZT	lead zirconate titanate
RMS	root mean square
TAW	traveling acoustic waves
SAW	surface acoustic waves
USW	ultrasound standing wave

1. Introduction

Lab on a chip (LOC) is a technology that combines several scientific fields and aims at the miniaturization of the real lab functions by integrating them into a single chip. The main aim of LOC technologies is point-of-care diagnostics: miniaturized versions of existing of existing assays, e.g., HIV testing,[1] fertility testing,[2] and cancer diagnostics.[3] Also, applications such as drug testing/delivery e.g. patient-specific drug test through a miniaturized chip, where a particular drug will be tested for an individual patient without the direct participation of the patient.[4] There are several advantages of such devices for this kind of applications: cost-effectiveness, fast response time and feasibility of parallelizing multiple processes.[5]

LOC is a subtopic of the more general field of microfluidics. Microfluidics is the science of designing, formulating and manufacturing devices, which handle liquids and/or gases at small length scales. Typical microfluidic devices have an overall device area of several square millimeters, and the fluid volumes used are in the order of microliters, nanoliters or even picolitres. Examples of broader applications of this research field includes food and environmental analysis, drug delivery studies, development and studies of biochips, ink-jet printers and more.[6]

The potentials and the bioanalytic applications of the lab on chips are not yet fully explored. Currently, several LOC bioanalytics applications require the integration of active materials to perform various actions, which includes micro-mixing of an aqueous solution, particle separation, from a flow stream, and particle alignment for imaging.[7,8] Currently, this has been achieved by using methods where the particles in aqueous solution are in direct contact with the actuation mechanism, or so-called *contact methods*. This has led to the integration of active components within a passive chip, which creates the need for designing application-specific structures compatible with the actuation medium. Due to the numerous fabrication steps and techniques involved, the fabrication costs and fabrication time increases rapidly. It would be preferable to have the actuation method outside the chip, and energy of the actuator transferred into the chip to manipulate flow streams, particles or cells inside the chip. This approach could be called *noncontact method*.[8] Noncontact manipulation reported in the literature includes dielectrophoresis, magnetophoresis, and surface acoustic waves. Dielectrophoresis is a phenomenon where manipulation of particles is achieved by a force exerted on a dielectric particle when is subjected to a non-uniform electric field.[9] This phenomenon can be used to separate particles using an electric field. In magnetophoresis, a magnetic force is used to manipulate magnetic particles through the microfluidic structure.[10] In acoustic manipulation, particles move in response to their interaction with acoustic waves. Acoustic manipulation can be achieved by using surface acoustic waves or bulk acoustic waves. One of the most researched applications of acoustic waves is separating particles in a continuous flow microfluidic channels.[11]

Some of the non-contact manipulation methods have some significant drawbacks when comparing one with the other. Initially, dielectrophoresis requires the microfabrication of electrode arrays, which can be a complicated process for a complicated microchannel structure. Additionally, the applied electric field on such devices can produce heat[12] or even affect the viability of cells[13] subjected to a high amplitude electric field. Secondly, magnetophoresis requires paramagnetic or ferromagnetic particles such as iron-based particles, so that it is rather limited in terms of the particles that can be

manipulated. Thirdly, surface acoustic waves require microfabrication of interdigitated electrodes on piezoelectric materials which is also a complicated process.

However, bulk acoustic waves have some attractive properties compared to the others: 1) There do not require microfabrication of electrodes, because commercial ultrasonic transducers can be used, where electrodes are pre-installed. 2) BAW transducers can in principle be decoupled from the microfluidic chip, making disposable chips more favorable and simpler in design. On the other hand, one major disadvantage of BAW, is the material requirements, such as high acoustic impedance. Such materials are glass and silicon, which make better acoustic resonators than plastics; however, fabrication of microfluidic chips on glass or silicon are typically more expensive to fabricate, and more time consuming.

In this thesis, bulk acoustic waves as a potential method for manipulating small particles (size ~ 100 μm) in microfluidic chips was studied. This thesis aimed to study if BAW acoustofluidic chips could be made out of hard plastic materials, instead of glass. Specifically, the thesis had two goals: a) use theory and numerical simulations to compare the behavior of acoustofluidics resonators made out of poly (methyl methacrylate) (PMMA), and Borosilicate glass; b) compare theoretical two-dimensional resonance patterns to experimentally obtained patterns. Initially, simulations have been carried out by COMSOL 5.2a Multiphysics package (COMSOL, 2012), to obtain numerical solutions for the devices' frequency response and their eigenfrequencies with the corresponding acoustic mode shapes for different materials. Then, the devices were fabricated out of PMMA and glass, and their actual frequency response (Appendix A) and acoustic mode characterization was done. In these experiments, polystyrene particles suspended in water were used to visualize the acoustic mode shapes. The motion of the particles was further tracked by particle tracking velocimetry (PTV). From the PTV data, we locate the resonant frequencies of the device, by finding frequencies for which the motion of the particles was significant for a given actuation amplitude.

The results obtained by simulations show that PMMA can be used as an acoustic resonator, due to its similar behavior with the simulated glass chip. However, by including the acoustic attenuation coefficient of the PMMA, the resonance frequencies of the lossy PMMA suffer significant pressure attenuation as the frequency increases, and frequency merging. The results of the lossy material are implementing that the higher the applied frequency the faster the pressure will decay, and thus very high frequencies will be hard to explore in PMMA. Additionally, preliminary experiments suggest that PMMA chip can be used in acoustofluidic micromanipulation, but the applied voltage should be far greater than the voltage applied in the glass resonator. This limits the operable spectrum of the PMMA chip in a multifrequency micromanipulation, due to the high voltage amplitudes required in the antiresonances of the device. it was also observed that the required voltages required were exceeding the maximum amplitude that the transducer could accept without taking any damage. Overfeeding the transducer with high voltage produced high temperatures during actuation, where the fluid starts to evaporate, and the particles are mostly affected by temperature gradients rather than acoustic forces.

2. Previous Work

In 1787, Ernst Chladni studied the motion of sand grains on vibrating plates with different geometrical shapes, which later have been widely known as Chladni plates. In his famous experiment, Chladni drew a violin bow across the edge of, for example a rectangular plate, at a point where a vibrational mode was excited, and he visualized the vibrational mode by the migration of sand grains to the nodal points on the vibrating plate.[14] In more recent years, scientists have adopted the idea of using sound waves to achieve particle motion within microfluidic channels.

Spengler, Coakley & Christensen[15] studied the acoustic phenomena induced by the formation of an acoustic standing wave within a micro-chamber. They reported acoustic microstreaming within an ultrasonic standing wave with polymer-based microparticles of sizes 1-25 μm. They observed that particles whose size was greater than 10 μm, were agglomerating at the pressure nodes as a result of the primary acoustic force. However, smaller particles were dragged by fluid flows induced by acoustic streaming.

Bengtsson & Laurell[16] studied the effects of acoustic streaming for fluid mixing and stirring in a dual flow single channel microfluidic device. The two separated flows where experiencing mixing due to Rayleigh streaming, induced by the acoustic wave dissipation through the bulk fluid. This particular result of their study introduced a new way to actively mixing fluids, while the integration of extra active components (actuators), and passive mixing structures were not needed. Thus, they reduced the dead volume of their device. The width of the microchannel was smaller than its length and comparable to a quarter of the acoustic wavelength. In addition, fluid stirring has been introduced in a 32-channel structure, in order to increase the enzymatic reactions taking place on the chamber walls. The 32-channel device dimensions, in this case, were smaller than the quarter of the acoustic wavelength.

Petersson et al.[17] implemented a continuous separation of different particle types within a fluid suspension, by the use of sound standing waves. The device had a single inlet, where a mixed solution (blood contaminated with labeled lipids) was introduced. The separation was relying on the acoustic contrast factor of the cells, where particles with positive contrast factor were focused in the pressure node, while particles with negative contrast factor were migrating into the pressure antinodes. The separation was achieved by employing bulk acoustic waves (BAW) from an actuating piezoelectric transducer at the half wavelength resonance frequency of the microfluidic channel. They have reported 80% efficiency on separating lipids from the whole blood, while 70% red blood cells (RBCs) were separated and collected at the center outlet of a trident styled outlet.

Hagsäter et al.[18] studied the eigenmodes in an acoustic microfluidic chip using numerical methods, and experimentally visualized them. Their device consisted of a piezoelectric transducer, and a bonded Pyrex lid on a silicon microfluidic device. The microfluidic device was attached on the piezoelectric transducer by an adhesive layer. The materials used for fabricating the microfluidic device

were selected for their excellent acoustic properties, and for their negligible attenuation coefficients. The visualization of the acoustic modes was achieved by imaging 1 μm and 5 μm microsphere polystyrene tracers, using microparticle image velocimetry (micro-PIV) to track their flow during actuation.

Leibacher, Reichert & Dual[19] studied droplet handling (droplet acoustophoresis) by using the primary acoustic force induced by an ultrasonic transducer in a two-phase flow(oil-water). The two-phase system was constructed by a continuous flow of silicone oil, and water microdroplets produced by a T junction flow-focusing structure attached to the main microchannel. They have reported a successful method of handling microdroplets, by tuning the microfluidic device into its first resonance frequency, and further to its second harmonic. They stated that due to the difference in acoustic characteristics of oil and water, the primary acoustic force was affecting the water droplets due to their positive acoustic contrast. Thus, water droplets suspended in oil were placed at the pressure minimum points formed across the microfluidic channel. Similarly, Fornell et al.[20] studied the effects of the primary acoustic force to manipulate particles within water droplets, in a similar two phase flow device. They formed water droplets by a T junction, and their size was comparable to the width of the channel. Standing waves were established between the channel walls at resonance frequencies, and the particles were forced to migrate at nodal points within the water droplets. At the end of the microfluidic device, a passive droplet splitter structure was used to split the water droplet into three daughter droplets while keeping the particles focused in the main droplet. The splitting process maximized the particle concentration in the center or to the two side droplets. This method established an effective way to minimize the waste volume of the buffer, and it has increased the concentration of particles exiting the outlet.

Lenshof et al.[21] discussed several fundamental criteria in order to design and build acoustofluidic resonators for trapping microparticles. In this article, several materials have been discussed such as silicon, glass-Pyrex, poly-(methacrylate)(PMMA), polydimethylsiloxane (PDMS), for their acoustic properties and compatibilities with the three types of resonators presented in their survey. Their study showed that polymer materials due to their high sound attenuation properties are not suitable for particle trapping in resonators actuated by bulk acoustic waves (BAW). However, in the same study was showed that surface acoustic wave resonators support the usage of polymer fabricated microchannels, due to the different method used to establish standing waves. It can be observed, that particle manipulation studies in acoustofluidics were mainly conducted in materials that have high acoustic impedance and low sound attenuation. Additionally, existing transversal acoustofluidic devices are mainly composed of silicon layer bonded on glass top lid, or by a glass channel bonded on a glass lid, but few studies have been reported similar results in transversal resonators based on polymer materials (polystyrene).

Savage, Burns & Fiering[22] implemented an acoustically actuated polystyrene microfluidic chip for plasma separation from the blood. In their study, the microfluidic chip was fabricated using rapid prototyping precision milling. Their experiments showed cell focusing in the middle of the polystyrene channel at an actuation voltage of 102 V and 0.125 mL/min volume flow. Similarly, Silva et al.[23]

performed separation of red blood cells from bacteria in a polystyrene acoustic microchannel with a trifurcated outlet. The polystyrene microfluidic chip has been fabricated using CNC, where it was thermally bonded with another polystyrene layer. Additionally, to the cell separation, Silva et al.[23] showed the relationship of the particle focusing width in their chamber with the supplied power. A simple observation of their results shows that the greater the applied power, the better the cell focusing and the thinner the focusing width becomes. In this thesis work, laser milling was used to fabricate a PMMA acoustofluidic chamber for particle micromanipulation applications. In addition, simulations and experiments were performed to charachterise the performance of a plastic (PMMA) acoustofluidic resonator compared to a glass chip for particle micromanipulation studies. Similar work has not reported in earlier studies.

3. Theoretical Background

3.1 Acoustic Theory

The linearized wave equation which describes the propagation of waves through an inviscid fluid is

$$\nabla^2 p = \frac{1}{c^2}\ \frac{d^2 p}{dt^2} \tag{1}$$

where ∇^2 is the Laplace operator, p is the pressure perturbation from the equilibrium pressure (units: Pa), c is the speed of sound (units: m/s), and t is the time (units: s).

The wave equation is derived by combining both the equation of mass conservation and momentum conservation (Navier-Stokes equation), and then considering small perturbations near equilibrium pressure and assuming inviscid fluids. In one dimension, the general solutions are $p = p(ct \pm x)$. Assuming time-harmonic fields ($p(x,t) = p(x)e^{-i\omega t}$) (1) becomes the (undamped) Helmholtz equation[24,25]

$$\nabla^2 p = -k^2 p \tag{2}$$

where $k = \omega/c$ is the wavenumber. For the case of acoustic manipulation, standing waves must be formed along a finite length device with certain boundary conditions such as a perfect reflector. When the wall material has a very high acoustic impedance $Z = \rho c$ (units: MRayls) relative to the acoustic impedance of the fluid, the boundary conditions can be assumed as a sound hard wall.

$$\mathbf{n} \cdot \nabla p = 0 \tag{3}$$

where **n** is the unit normal of the interface. The solution of the Helmholtz equation using the hard wall boundary conditions results in a standing wave, which in the case of a rectangular cuboid chamber, becomes

$$p_{n_{x,y,z}} = A \cos\left(\frac{n_x \pi}{L_x} x\right) \cos\left(\frac{n_y \pi}{L_y} y\right) \cos\left(\frac{n_z \pi}{L_z} z\right), n_{x,y,z} = 0,1,2, \ldots \tag{4}$$

where A is the amplitude of oscillation, and $n_{x,y,z}$ are the mode numbers in x-, y-, and z-direction, and $L_{x,y,z}$ are the dimensions of the chamber. Inserting (4) in (2), and by substituting $k = 2\pi f/c$, the eigenfrequencies of the rectangular cuboid can be computed by

$$f_{n_{x,y,z}} = \frac{c_{\text{fluid}}}{2} \sqrt{\left(\frac{n_x}{L_x}\right)^2 + \left(\frac{n_y}{L_y}\right)^2 + \left(\frac{n_z}{L_z}\right)^2} \tag{5}$$

For the case of a thin resonator where $L_z \ll L_{x,y}$,and subsequently $f \ll f_{0,0,1}$, the 2D -dimensional resonant frequency can be calculated by

$$f_{n_{x,y}} = \frac{c_{fluid}}{2}\sqrt{\left(\frac{n_x}{L_x}\right)^2 + \left(\frac{n_y}{L_y}\right)^2} \tag{6}$$

We previously discussed the standing wave pressure field in eq. (4), for devices with sound hard boundaries, where their resonant frequencies can be calculated by eq. (5). Similarly, for sound soft boundaries the pressure at boundaries is:

$$p = 0 \tag{7}$$

, where the pressure field within the chamber becomes as:

$$p_{n_{x,y,z}} = A\sin\left(\frac{n_x\pi}{L_x}x\right)\sin\left(\frac{n_y\pi}{L_y}y\right)\sin\left(\frac{n_z\pi}{L_z}z\right), n_{x,y,z} = 1,2,3\ldots \tag{8}$$

The difference of the sound soft boundaries is that the pressure fields are developed right away from the walls ($0 < \mathrm{x,y,z} < \mathrm{L_{x,y,z}}$).

In this thesis work, we are not only involving sound hard materials such as glass, with high acoustic impedance ratio Z_r, but also plastic PMMA and soft PDMS elastomer. The boundary conditions at the fluid-wall interfaces can be assumed by the impedance ratio of the materials. [28]

$$Z_\mathrm{r} = \frac{Z_\mathrm{chip}}{Z_\mathrm{fluid}} \tag{9}$$

A) $Z_\mathrm{r} \gg 1$: At the limit of $Z_r \to \infty$, the liquid-chip interfaces behave like sound hard boundary conditions. However, as it will be shown in the results, even glass chips cannot be treated as having infinite acoustic impedance, because the impedance of water $Z_\mathrm{water} \cong 1.5\ \mathrm{MPa\ s\ m^{-3}}$ while the surrounding medium glass has an acoustic impedance of $Z_\mathrm{glass} \cong 13\ \mathrm{MPa\ s\ m^{-3}}$, which yields only to $Z_\mathrm{r} \cong 8.66$.[26]

B) $Z_r \ll 1$: At the limit of $Z_\mathrm{r} = 0$, the chip-liquid interface can be treated as a soft wall boundary conditions will be assumed for the fluid-solid interface. However, even for PDMS, the PDMS-water impedance ratio results $Z_\mathrm{r} \cong 0.68$, which is closer to unity than zero.

C) $Z_r \approx 1$: In this general case, the propagation of the wave in the chip has to be considered. The wave will be partially reflected and partially transmitted from the fluid-solid interface and the whole geometry of the chip has to be considered.

These boundaries (soft and hard) are then implemented in simulations to visualize acoustic patterns by computing the natural frequencies using Helmholtz equation eq. (2). The results of such simulations are giving out theoretical frequency values, similarly by solving eq. (6) for a thin resonator, whereas simulation results provide the corresponding eigenmodes of such device at resonances. In

the actual simulation study of the acoustofluidic device, damping of the vibrating chip, and sound energy losses due to the viscosity of the fluid are neglected.

3.2 Manipulation of Particles in Acoustofluidic Devices

Acoustofluidic microdevices are microfluidic devices where manipulation relies on the use of the ultrasonic standing waves (USW), traveling acoustic waves (TAW), bulk acoustic waves (BAW) or surface acoustic waves (SAW). In the BAW case as in this thesis, ultrasonic standing waves are excited from a transducer and are imposed on the fluid through excitation of the microchannel walls.[27] Firstly, primary acoustic radiation force (F_P) appears in the particle suspension, which results from the particle-wave interaction. Acoustic waves interact with a particle, which typically has a higher speed of sound than the surrounding fluid. The wave exerts a force on the particle because of the difference in the acoustic properties of the two materials. Secondly, acoustic streaming results from a traveling wave getting attenuated by the fluid's viscosity. Acoustic streaming appears as a fluid flow and the particles experience a drag force in the direction of streaming. Lastly, there is secondary acoustic radiation force (F_S, also known Bjerknes force), which is an attractive or repulsive particle-particle interaction. Secondary acoustic radiation force originates from the scattered pressure field, radiated by an oscillating particle or a bubble. The effect of F_S can be visualized whenever the particles have been exposed to F_P: F_S is responsible for the particle clustering.[28]

3.2.1 Primary Acoustic Radiation Force

The primary acoustic radiation force (F_P), is the force induced by the scattering of ultrasonic waves on suspended particles in the fluid. Particles, cells and different types of fluid emulsions, tend to migrate at lower or higher-pressure points, the so-called pressure nodes or pressure antinodes. The trajectory of the exposed particles has a strong depence on e.g. the particle's density and compressibility, and size in the case of multi sized particle suspension. This particular force relies on momentum transfer from the ultrasound standing waves to the suspended particles whose position exhibits a translational movement. This force was first described by King,[29]Yosioka,[30] and later by Gor'kov.[31] In this thesis, we adopt the Gorkov's approximation of the primary acoustic force, which is identical to the force reported by Yosioka in one dimension for a freely suspended particle within a non-viscous fluid. Gorkov approximated the primary acoustic force as

$$F_P = 4\pi a^3 \Phi k E \sin(2kx), \text{ where } k = 2\pi/\lambda, \Phi = \frac{b_{\text{fluid}} - b_{\text{particle}}}{3b_{\text{fluid}}} + \frac{\rho_{\text{particle}} - \rho_{\text{fluid}}}{2\rho_{\text{particle}} + \rho_{\text{fluid}}} \quad (10)$$

where a is the radius of the particles (units: m), Φ is the acoustic contrast factor (unitless), k wavenumber (unit: rad m^{-1}), E the acoustic energy density (units: J m^{-3}),x direction of wave propagation, $b_{\text{fluid,particle}}$ the isentropic compressibility of the fluid (units: Pa^{-1}), and $\rho_{\text{fluid,particle}}$ are the densities of both fluid and particles respectively.[32,33] The acoustic contrast factor Φ in eq. (10), determines if the particles will migrate towards or away from the pressure nodes. If $\Phi > 0$, the particles tend to move towards pressure nodes (pressure minimums), while for $\Phi < 0$, the particles move towards pressure antinodes (pressure maximums). In this thesis polystyrene particles will be used to visualise the pressure minimums of the acoustofluidic device, because their acoustic contrast factor was found to be $\Phi = 0.193$.

The acoustic energy density E, scales with the square of the applied voltage on the piezoelectric transducer ($U_{p-p}{}^2$).[33] Using this relationship of the applied voltage and the acoustic energy density, one can estimate the acoustic force applied to a spherical particle with radius a, up to a scaling coefficient. Unfortunately, the scaling coefficient depends on the geometry and applied frequency, so that detailed simulations and experiments are still needed.

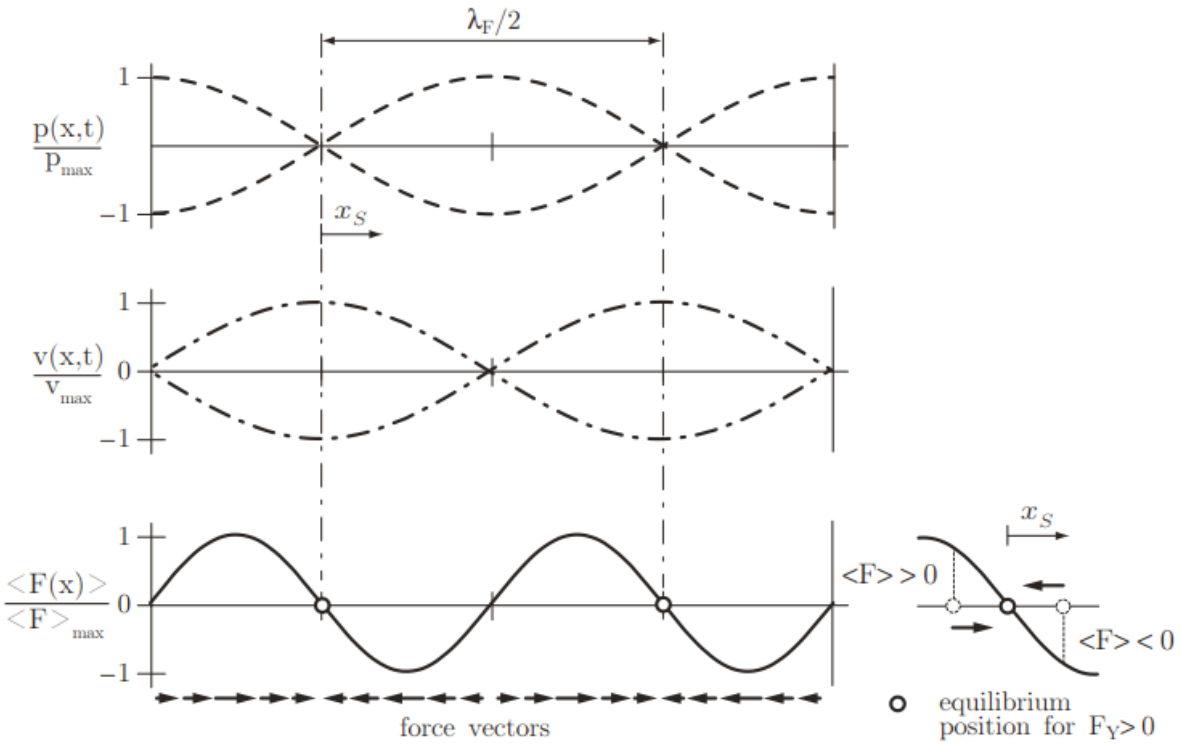

Figure 3.1. Full wavelength pressure and velocity fields induced by an acoustic standing wave within a fluid cavity. Acoustic force vectors indicating the trajectories of the particles from the positive and negative directions of the nodal points, when their acoustic contrast factor is positive.[34]

3.2.2 Acoustic Streaming

Acoustic streaming is a fluid formed stream, induced by viscous dissipation of acoustic energy into the boundary layer of the fluid, and any solid boundary, that is comparable or greater than the quarter of the acoustic wavelength.[35] In ideal case, when the viscosity of a fluid is equal to zero, acoustic streaming will not be presented.[36] Since ideal fluids are hard to find in nature, this phenomenon will occur, and it can be visualized in the form of steady vortices nearby the boundaries.

Streaming flows are observed in fluid cavities, where at least one dimension of the cavity is perpendicular to the direction of the acoustic wave, and its dimension is comparable or greater than the acoustic wavelength.[35] Fluid flows in the form of vortices is initialized from the boundaries, due to the larger dissipations of acoustic energy on the boundaries rather than in the bulk, which will form a steep velocity gradient perpendicular to the acoustic wavelength. The width of the boundary vortices δ is given by

$$\delta = \sqrt{\frac{2\nu}{\omega}} \tag{11}$$

where ν is the kinematic viscosity of the fluid (units: $\mathrm{m^2 s^{-1}}$), and ω is the angular frequency (units: rad $\mathrm{s^{-1}}$). From (11), we see that δ decreases as the angular frequency increases. This frequency dependence of δ in the case of a multifrequency acoustofluidic device, where its operational frequencies are not restricted only on the first harmonics, can vary with any frequency change. Then the width of the boundary streaming has a tunable size and can become tiny compared to the overall dimensions of the device. Typically for water in MHz range, δ is less than 1μm.[37] The lowest frequency used in the manipulation experiments in this thesis work was 60 kHz, so that $\delta = 68.86$ μm. The lateral dimensions of the devices used in this thesis are 10 mm, and the thickness of the fluid is chamber is 440 μm, so it is reasonable to assume that the width of the boundary streaming is negligible in the lateral directions, but not necessarily so in the z-direction.

Additionally, in the presence of USW in the acoustofluidic chip, streaming of the bulk fluid follows, also known as Rayleigh streaming, which forms vortices of width equal to quarter the acoustic wavelength. Rayleigh streaming named after Lord Rayleigh who studied the acoustic streaming phenomena of spherical particles in fluids.[38] Figure 3.3 illustrates the streaming patterns formed in an acoustofluidic device when a half-wavelength standing wave is established along the microchannel, where $\delta \ll h \ll \lambda$. δ is the boundary streaming width, h is the height of the channel, and λ is the acoustic wavelength.

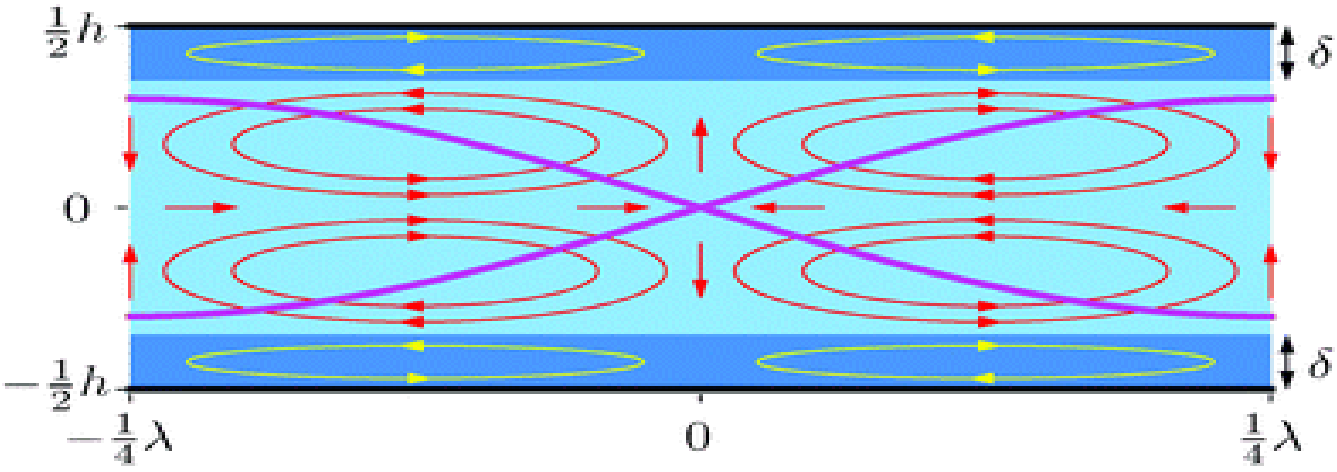

Figure 3.2. Acoustic streaming within an acoustofluidic channel, where black color represents infinite parallel rigid walls, dark blue the boundary streaming layer δ, Schlichting streaming yellow vortices, and light blue color represents the bulk fluid with quarter wavelength size Rayleigh streaming patterns. [38]

Particles experience a drag force in a fluid with streaming induced flows. The drag force for a spherical particle is given by the Stokes' drag equation

$$F_{\mathrm{drag}} = -6\pi a\eta v \tag{12}$$

where a is the radius of the particle (units: m), η is the dynamic viscosity of the fluid (units: Pa s) and fluid velocity v (units: m $\mathrm{s^{-1}}$). Provided that all the acoustic fields and fluid flows are known, we can use $F_{\mathrm{drag}} = F_{\mathrm{P}}$ to find the minimum particle size that can be manipulated using the primary acoustic radiation force.[39] Eq. (10)shows that the acoustic force F_{p}, scales with the particle volume, whereas

F_{drag} scales with the radius of the particles. Therefore, larger particles are expected to be easier to manipulate by F_{p}. Furthermore, choosing a less viscous fluid means that both η and v in eq. (12) are decreased, thus F_{drag} is decreased. The streaming patterns will also change, as it can be seen in eq. (11) that fluids with smaller kinematic viscosity will induce smaller vortices.[39]

3.2.3 Secondary Acoustic Force

Secondary acoustic force (F_{S}), arises in the presence of particles or bubbles, which is the case in most acoustofluidic manipulation setups. When sound waves interact with particles, F_{P} forces the particles to migrate to pressure nodes/antinodes (e.g. towards the nodes when $\Phi > 0$). F_{S} then appears due to the scattered sound field on a particle and affects the nearby particles. The secondary acoustic force F_S for two identical spherical particles interacting with a one-dimensional plane wave is given by[20]

$$F_{\text{S}} = 4\pi\alpha^6 \left[\frac{(\rho_{\text{particle}} - \rho_{\text{fluid}})(3\cos^2\theta - 1)}{6\rho_{\text{fluid}} d^4} V^2(x) - \frac{\omega^2 \rho_{\text{fluid}} (\beta_{\text{particle}} - \beta_{\text{fluid}})}{9d^2} p^2(x) \right] \quad (13)$$

where d is the distance interconnecting the centers of two nearby particles (units: m), α the particle radius (units: m), ω is the angular frequency (units: rad s^{-1}), and θ is the angle of the line connecting the centers of two particles, and the direction of the incident wave. $V(x)$ and $p(x)$ are the velocity and pressure fields of the unperturbed incident field on the particle's position, $\beta_{\text{particle,fluid}}$ the compressibility of the particle and the host fluid medium, and $\rho_{\text{particle,fluid}}$ are the densities of particles and the density of the fluid. This force can be attractive, meaning that particles will create clusters when exposed to F_{S}, where the repulsive case results whenever the sign of F_{S} is negative. [20,40]

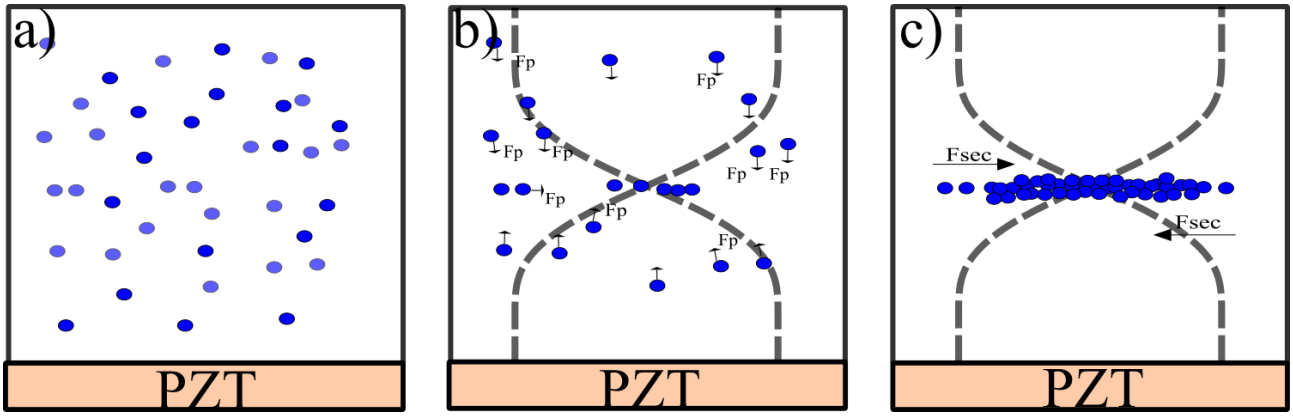

Figure 3.3. a) Particles suspended in fluid where ultrasound is off. **b)** Particles migrating to Pressure node due to the primary acoustic force. **c)** Particles clustering in the pressure node due to the effect of secondary acoustic force. [42]

3.3 Summary

It is important here to highlight the significant effects of the forces exerted on particles in a standing wave field. Each acoustic force interacts with particle suspension differently, where the direction of particle motion is related to the frequency and the on the displacement amplitude of the pressure field. Firstly, the primary acoustic radiation force F_{P} interacts with particles in the suspension by pushing the particles towards either pressure nodes or antinodes depending on their acoustic contrast factor.

Secondly, there are the effects of acoustic streaming, which induce a drag force on particles. This drag force scales with the particle radius, which in the case of some micron meter particles this force will dominate over F_{P}.

If acoustic streaming dominates, then the effects of the primary acoustic force on particles will be negligible, and the particle suspension will experience a force induced from the fluid flow F_{draq}, where particles will follow the direction of the fluid streams. Since primary acoustic force F_{P} scales with the volume of the particle and F_{drag} scales with particle radius, an increase in the particle radius will result to a larger magnitude of F_{P}, which will eventually dominate the effects of acoustic streaming.

Lastly, the secondary acoustic force F_{S} appears due to the harmonically oscillating acoustic pressure field scattered from individual particles in the particle suspension. The scattered pressure field then results to a particle-particle interaction which can be a repulsive or an attractive motion between particles. The magnitude of F_{S} scales with the square of the particle volume, which in the case of some micrometer particles is very small and can be neglected.

In acoustic particle manipulation, the particle or particles should experience a force that have a defined direction and amplitude. In this view, both primary acoustic force and acoustic streaming seem favorable for acoustofluidic manipulation, because they depend mainly on the device geometry. On the contrary, the secondary acoustic force affects the relative positions of particles, so it seems to be less favorable for controlled manipulation.

4. Materials and Methods

In this thesis work, we fabricated acoustofluidic chips from two different materials: PMMA and glass. The design and fabrication of these chips are detailed in Sections 4.1 and 4.2, respectively. Section 4.3 describes the particle tracking velocimetry used to track particle movement inside the chips, and Section 4.4 describes the methodology used to distribute the particles evenly inside the chamber. Finally, section 4.5 details the simulations that were done using COMSOL Multiphysics software, and section 4.6 discusses details the methodology used to carry out preliminary experiments.

4.1 Design of a Two-Dimensional Acoustofluidic Resonator

Traditionally, acoustofluidic chips reported in literature were fabricated out of materials with high acoustic impedance, such as glass ($Z \cong 13$ MPa s m^{-3}), or silicon ($Z \cong 19$ MPa s m^{-3}).[21] We wanted to test if hard plastics could still be used. Out of common engineering plastics, PMMA has a relatively high acoustic impedance ($Z \cong 3$ MPa s m^{-3}) compared to other plastics, such as polyethylene ($Z \cong 1.73$ MPa s m^{-3}),[42] and polycarbonate ($Z \cong 2.69$ MPa s m^{-3}).[44] For this thesis work, an acoustofluidic chip made from glass was selected as a reference material, due to its high acoustic impedance, which is much higher than the acoustic impedance of PMMA (Table 1), and has negligible attenuation coefficient. In addition to the high acoustic impedance of glass, glass has high optical transparency, thermal resistance, dimensional stability, and chemical inertness. On the other hand, PMMA was chosen for its moderate acoustic impedance, transparency, rigidity, dimensional stability, which are suitable for the nature of the experiments followed in this thesis. Unlike glass, PMMA was considered an acoustically lossy material, due to its large attenuation coefficient.[21,43,44] In contrast to the fabrication processes of silicon and glass, the fabrication processes of polymer-based devices by materials such as PDMS, and PMMA are numerous, involving rapid prototyping methods. Some of this methods are injection molding, hot embossing, 3D printed molds for elastomer casting, direct laser milling.

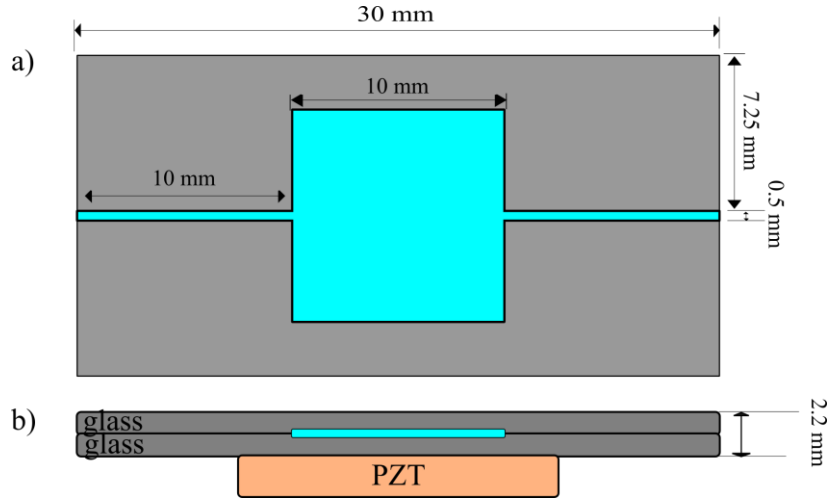

Figure 4.1. Design and dimensions of the glass acoustofluidic devices. **a)** Top view of the 10 mm × 10 mm ×0.44 mm chamber with side inlets. **b)** Cross section of the device and the coupled PZT transducer.

Table 1. Properties of the materials used in the acoustofluidic chips in this thesis.

Material Name	Speed of sound c [m s^{-1}]	Material Density ρ [kg m^{-3}]	Acoustic Impedance Z_{ac} [Rayls]	Attenuation coefficient a [dB cm^{-1}]	Reference
DI-water	1500	1000	1.500×10^6	-	21
PMMA	2590-2800	1150	2.978×10^6	~10@6MHz	44
PDMS	1076	965	1.038×10^6	~31@6.61MHz	44,45
Borosilicate glass	5500	2203	12.116×10^6	-	46
Polystyrene Particles	1700	1050	1.785×10^6	-	44

In Figure 4.1, the schematics of the glass acoustofluidic devices are shown. Two chips with a milled chamber of 10 mm × 10 mm × 0.22 mm are placed on top of each other, resulting in a chamber of 10 mm × 10 mm × 0.44 mm. This chamber serves as the particle manipulation area. The same schematic was used for the PMMA chip; however, the schematic was transferred only on one side of the PMMA substrate, resulting in a 10 mm × 10 mm × 0.2 mm chamber. The inlet and outlet of both chips were connected on two 3D printed structures that helped the tube inlet-outlet connections to the chips.

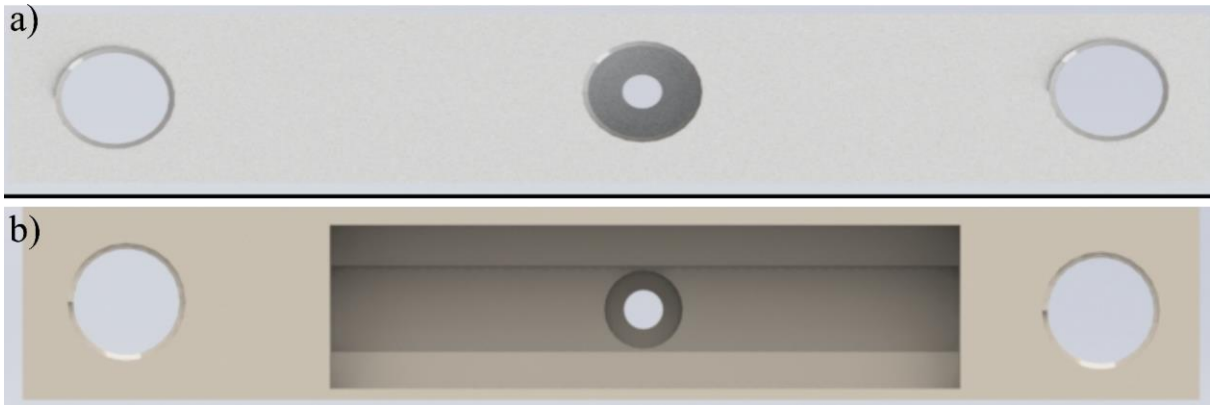

Figure 4.2. 3D printed chip holder with Inlet structures. **a)** back side of the structure, where a silicone tube of 1.5 mm inner diameter will be connected to the inlet. **b)** front view of the structure, where the connection of inlets/outlets on the chip occurs in the cavity of the structure.

The acoustofluidic chips were fluidically connected to the inlet and outlet tubes by using two inlet structures (Figure 4.2), where two screws were used to lock the devices and secure the structures on the chips. Furthermore, the inlet-outlet structures were connected to a syringe pump via a 1.5 mm inner diameter silicone tubes.

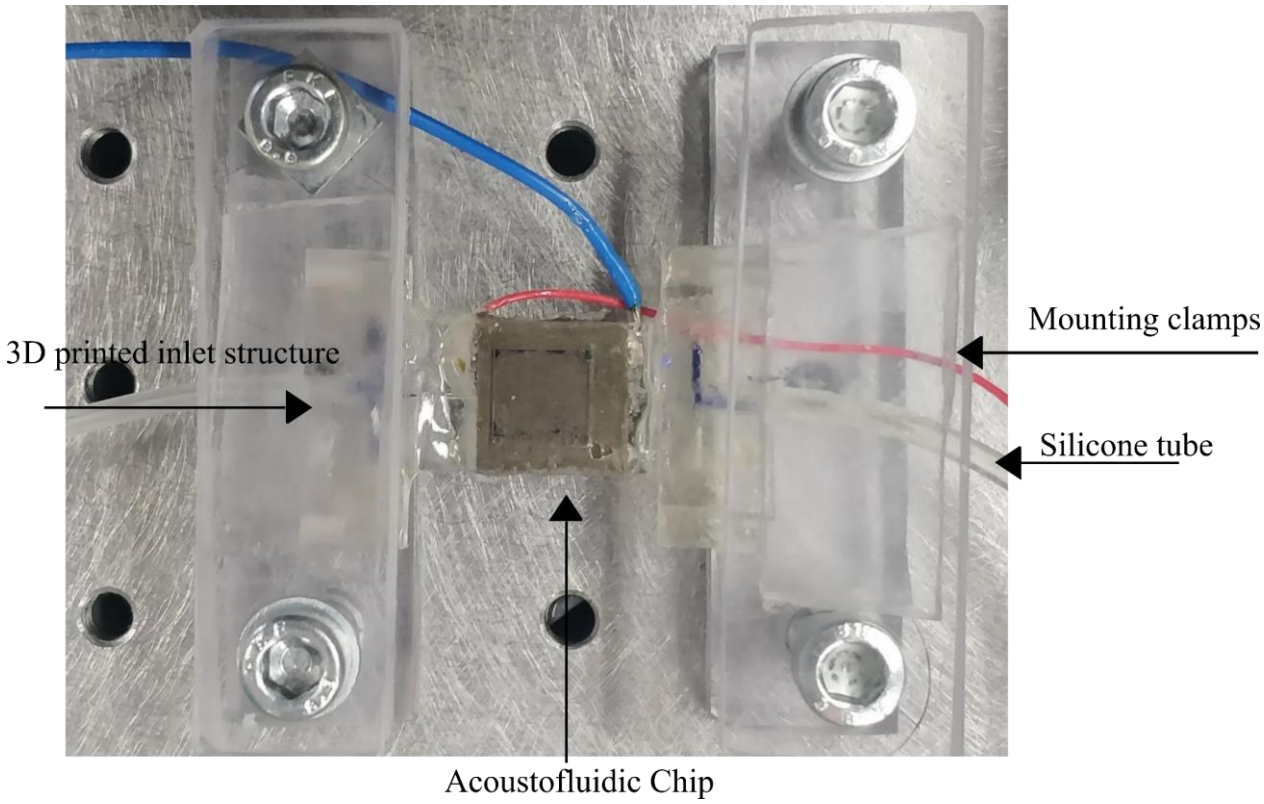

Figure 4.3. 3D inlet-outlet mounted structures on the glass acoustofluidic chip. Overall device mounted by locking clamps on top and bottom of the acoustofluidic chip, for a secure clamping of the device on the vibration free table.

The tracing particles such as polystyrene particles, can be used to visualize how standing waves are developing in the acoustic chamber, similarly to the sand grains in Ernst Chladni's experiments. Polystyrene particles were selected due to their positive acoustic contrast factor ($\Phi = 0.193$ in water). Thus, particles will tend to migrate to the acoustic nodes, forming acoustic patterns of the actuated frequency. These patterns can be used to compare the actual acoustic modes of the devices with the theoretical eigenmodes. Acoustic standing waves were established from the microfluidic chamber walls, through bulk acoustic waves induced by the piezoelectric transducer. This configuration is known as the acoustic transversal resonator,[21] and this configuration was employed in all the devices in this thesis work. The fabricated devices have followed the principles of fabricating this kind of resonator as shown by [21], where

$$Z_{\text{piezo}} > Z_{\text{channel}} \geq Z_{\text{reflector}} \tag{16}$$

and by attaching the piezoelectric transducer similarly to the Figure 4.1 above.

4.2 Microfabrication Procedures of the Acoustofluidic Devices

For this study, a polymer-based acoustofluidic device was fabricated out of PMMA, and another device was made out of glass, to compare the performance of the two. The PMMA chip was fabricated by laser milling of a 2 mm thick PMMA sheet, followed by thermal solvent-based bonding of a PMMA lid. The glass device was fabricated by femtosecond laser milling, and the device was thermally bonded.

4.2.1 Fabrication of PMMA Acoustofluidic Chip

The fabrication of the PMMA acoustofluidic chip was done using laser engraving. The engraving has been carried out by using the CO_2 Epilog fusion M2 32 laser. This fabrication method is fast and time-efficient for prototyping, compared to conventional cleanroom microfabrication. In addition, the number of chips that can be produced per batch is limited only by the engraving area (100 cm × 75 cm), which is much larger than the surface of silicon wafer used in the conventional microfabrication. For the fabrication of the PMMA chip, a PMMA substrate of $40\ \text{mm} \times 40\ \text{mm} \times 2\ \text{mm}$ was placed into the engraving area. Then the CAD drawing shown in Figure 4.1 was uploaded to the controller of the engraving machine using Adobe Illustrator.

Before starting the engraving, the power parameters (Table 2) were adjusted by trial and error to meet the requirements of our design. The engraving process was repeated two times with the engraving parameters set to high speed and low power (Table 2). This way the engraved area became smoother than the engraved area achieved from a single engraving cycle. As soon as the engraving/cutting process was done, both PMMA channels and top lid were cleaned using isopropanol and DI water prior to bonding. The depth of the engraved chamber was measured by stylus profilometry, where the depth was found to be approximately $180 \pm 30\ \mu\text{m}$.

Table 2. Epilog Laser Power and Speed Parameters.

	Engraving Power/speed Parameters	Cutting Power/speed Parameters	Engraved Depth per Repetition	Number of Engraving Cycles
PMMA Top lid	None	100W @ 1000DPI	4mm	1
Microfluidic structure	30W @ 1200DPI	100W @ 1000DPI	$\approx 100\mu m$	2

In the next step, the PMMA channels and top lid were bonded together, by applying a thin film of ethanol between the lid and the channels. The PMMA lid and channels were stacked and pressed together by pressure clamps and placed in a fan assisted oven. The temperature used for bonding the two PMMA parts was 68 ˚C, for a period of 15 minutes. In such a temperature, a solvent such as ethanol tends to dissolve a thin PMMA film over the attached pieces. When the solvent evaporates, the dissolved PMMA films are reconnected. The bonded pieces of PMMA were then taken out from the oven and let to cool for 5 minutes.[45]

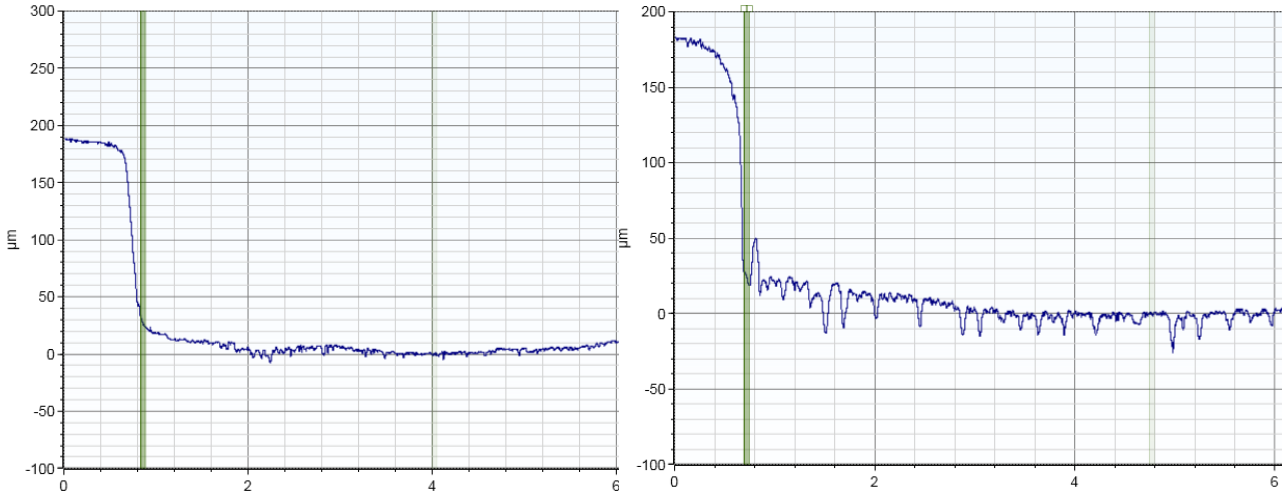

Figure 4.4. 2D Stylus Profilometry of the engraved PMMA chamber shown in Figure 4.5. The Engraved PMMA microfluidic chamber has overall dimensions of 10 mm × 10 mm × 0.18 ± 0.030 mm.

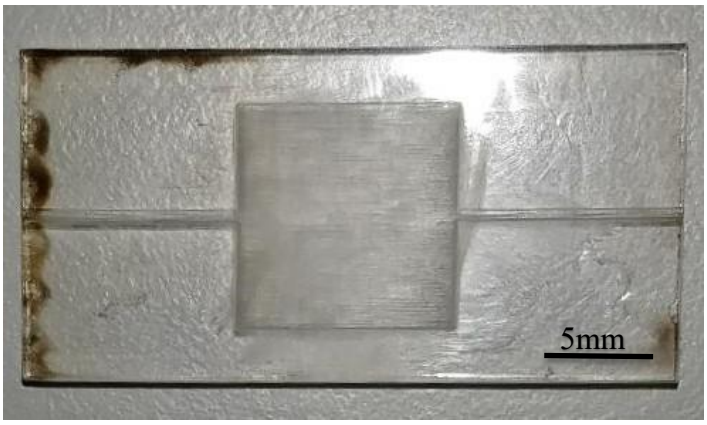

Figure 4.5. Laser engraved PMMA microfluidic chip.

The pressure clamps were removed as soon as the PMMA chip was cooled. The bonded channels, and lid are shown in Figure 4.6. In order to test the channels for leakages, blue dyed water was pumped to the channels and no potential leakages were found.

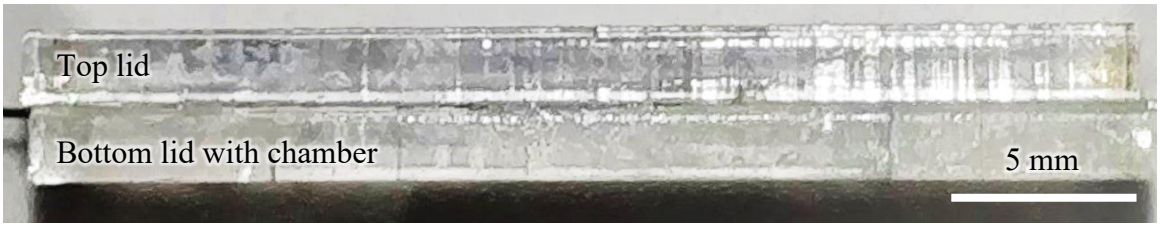

Figure 4.6. PMMA chip sideview. Top lid and bottom microfluidic structure bonded by using a thin layer of ethanol between both lid and channel for 15 minutes in an oven at a temperature of 68 °C.

4.2.2 Fabrication of Glass Acoustofluidic Chip

The glass chip was fabricated using femtosecond laser ablation, which is an accurate and fast prototyping method with the ability to create 3D features. For the fabrication, a 1.1 mm thick borosilicate

glass substrate was used. The femtosecond ablation on the glass substrate was performed on a laser workstation platform (microSTRUCT-C, 3D-Micromac, Chemnitz, Germany), equipped with a Yb: KGW solid state laser, with a maximum average power of 15 W, and laser wavelength of 1030 nm. The femtosecond ablation was done by our collaborators (Kai Mattern, working under the supervision of Prof. Andreas Dietzel, at the Technical University of Braunschweig).

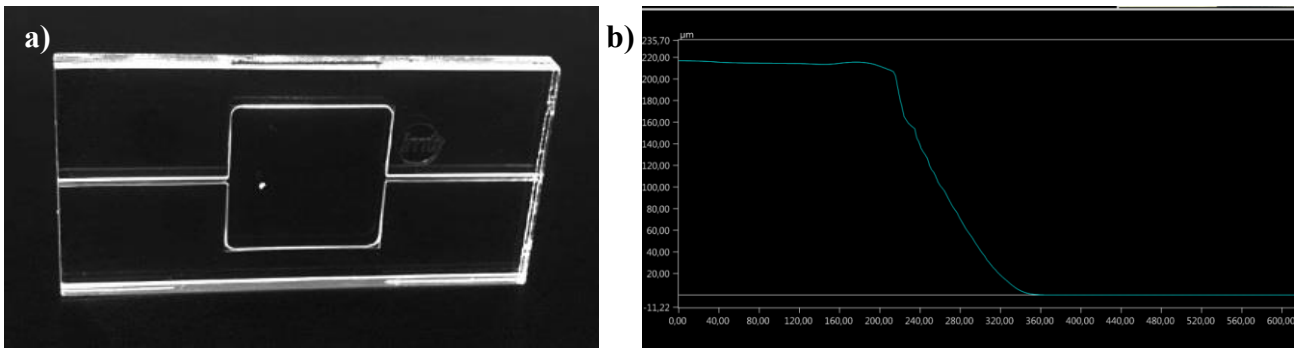

Figure 4.7. a) Thermally bonded glass microfluidic structures with glass top lid, **b)** Profilometry of the glass chamber. The depth achieved on each glass piece using femtosecond laser ablation is ~220 µm, with total chamber depth of 440 µm.

Due to the extreme high energy densities at a very short period of every pulse, the materials show no absorption at that wavelength and make femtosecond laser 3D structuring possible. Using this method the borosilicate glass channels were fabricated, where later they have been dipped into Hydrogen Fluoride (HF) to improve surface smoothness, and then bonded with the second borosilicate channel structure by using thermal bonding. [46]

4.3 Particle Tracking Velocimetry Analysis and Eigen Mode Visualization

Particle tracking velocimetry was employed in the experiments to track individual particles at any time that the acoustofluidic device was actuated. Using PTV, we were able to visualize how particles flow at any excitation frequency, and thus, we are able to reconstruct the acoustic pattern for that frequency. PTV was achieved by detecting individual particles using a machine vision camera, and MATLAB's Image acquisition toolbox. Particle detection was achieved by image processing of the acquired frames, where we were identifying individual particles by matching their color (blue), and size (13 pixels per particle;13pixels=100µm). The imaging area was set to10 mm × 10 mm, while particle tracking was performed on ten frames in the amplitude scanning experiments. The detected particles were matched in each frame, by using a matching algorithm. Furthermore, the obtained motion plots were compared with the acoustic mode shapes, obtained by simulations carried out by COMSOL Multiphysics software.

4.4 Particle Mixing and Mixing Distribution Efficiency

Particle mixing within the acoustofluidic chamber was accomplished, by employing acoustic waves at frequency close to the first, and second acoustic resonant frequency for the PMMA acoustofluidic chip at high amplitudes. The mixing of microparticles is a result of acoustic streaming, where induced

drag flows at high velocities, dragging the particles in the flow stream, and as a consequence breaking formed clusters and spread the particles within the chamber. However, in the glass chamber a different procedure was followed, where a frequency of 1.022 MHz@100mV ($n_x \cong 10, n_y \cong 10$) was used to align the particles in the chamber. Acoustic streaming was not always achievable in the glass chamber (sometimes worked, sometimes a pattern was formed), and thus particle alignment in multiple lines, was an equally effective way to 'mix', rearrange the particles in the chamber.

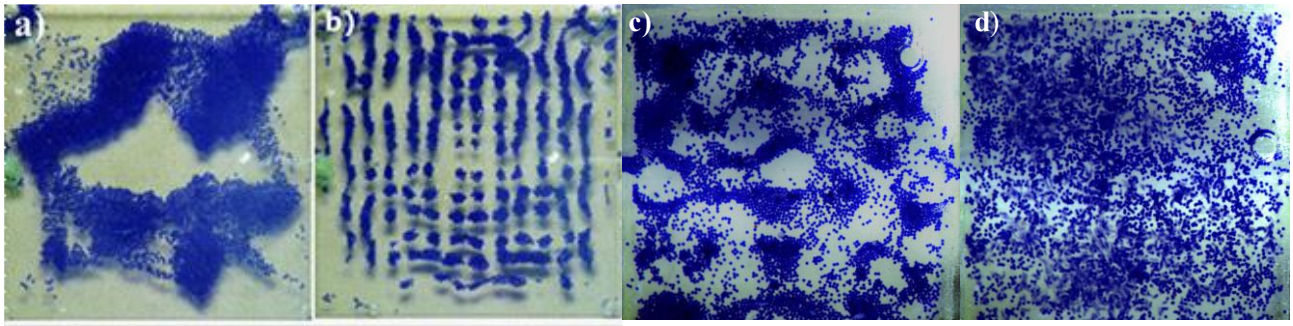

Figure 4.8. 'Mixing' of polystyrene particles within **a-b)** glass acoustofluidic chamber. **a)** shows the particle clustering within the chamber, whereas **b)** shows the particle spreading and alignment by using 1.022MHZ@100mV from waveform generator. Similarly, **c-d)** show mixing within PMMA **c)** at 65kHz@115 mV, where **d)** show the spread particles right after mixing.

In order to calculate mixing efficiency, two images (before and after mixing) were used as in Figure 4.8. Initially, the image before any mixing process was scanned by the particle tracing software, where the number of particles and their location was recorded. The same procedure was followed for the second image, which is the first image captured after the mixing process. chamber was divided into 2 × 2 bins and a 2D histogram of the particle counts within each bin was computed. The uniformity/randomness of the particle distribution was tested by using Chi-squared method. Ideally if the chi-squared results in a value higher than 0.05 then the mixing process results into a statistically random-uniform particle distribution, whereas for a value less than 0.05 the particle distribution is not statistically random.

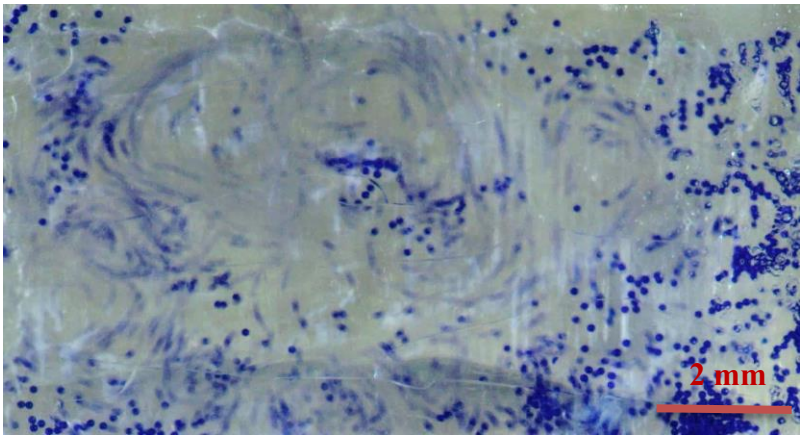

Figure 4.9. Mixing of polystyrene particles via acoustic streaming within the PMMA chamber.

4.5 Acoustic Simulations

Acoustic simulations were carried out using COMSOL Multiphysics finite element package. Simulations have been done to determine the acoustic response of the acoustofluidic chamber in three cases, where the variable component was the enclosing material of the device. This three-case simulation aims to determine which material is 'best suited' for the aim of this study. In COMSOL, the selected physics was Pressure Acoustics- Frequency domain, found in the acoustics module, and the selected studies were eigen frequency and Frequency Domain. The frequency domain module of pressure acoustics, models the problems using the modified Helmholtz equation.[47]

In the case of eigen frequency study the eq. (2) is solved. The solver of COMSOL solves an eigen-value problem in order to determine the natural frequencies nearby a selected frequency.

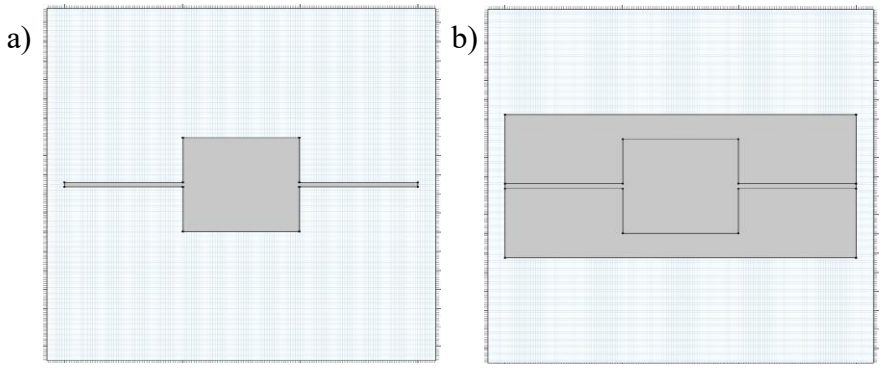

Figure 4.10. 2D COMSOL CAD for PMMA, PDMS, and Glass. **a)** Fluidic channel and chamber, **b)** full chip model.

Different boundary conditions can be added to accurately describe the interaction of soundwaves propagating from a solid material to the fluid in the chamber. Initially in the eigen frequency study, we will model only the fluidic channels and chambers without the surrounding glass material. The channels and chamber walls will be modelled by using the assumption of sound hard walls for glass, and PMMA, resulted from the calculation of their impedance ratio as in eq. (9). Since the impedance ratio of both PMMA and glass will be greater than one ($Z_{\mathrm{PMMA,glass}} > 1$), the chamber walls can be modeled as sound hard boundaries, while the inlet and outlet of the device will be modeled as sound soft boundaries (water-air interface). Secondly, the full chip (Figure4.10 b)) model with different enclosing materials will be modelled with sound soft boundaries at the outer boundaries, while the fluidic boundaries will be modelled by pressure continuity boundary conditions. The resulted eigenfrequencies of the chamber will be then compared, with eigenfrequencies of the full chip model with variable materials.

Additionally, a frequency domain study will be studied, for the full chip model by using the following enclosing materials: PMMA, PDMS, and glass. The excitation of the acoustic waves was taken care by a monopole sound source. The monopole sound source was used because it has the ability to emit a uniformly strengthen acoustic field within the chamber. The amplitude of the monopole source was set to an arbitrary $Q_{\mathrm{m}} = 1\mathrm{s}^{-2}$, because the equations are linear, and we are mainly interested in the frequencies and relative amplitudes of the resonance peaks, not their absolute amplitude. The frequency range used in this study was $30-500$kHz with 1 kHz frequency increments. Two different meshes were used in each of the 2D models, to improve the accuracy of the numerical solution, and to reduce computational expenses. The mesh size for the fluid chamber and channels has been set to

200 μm with 4978 triangular mesh elements, whereas the rest was a quad mesh with 1616 meshing elements of 2 mm.

4.6 Sample Preparation, Experimental Setup

The sample used in the experiments was polystyrene particles diluted in Triton X-100 (10% in DI-water). The polystyrene-Triton sample contained 0.5 ml of 100 μm polystyrene particles, and 9.5 ml of water-Triton X-100 solution. The addition of Triton X-100 reduced the tendency of polystyrene particles to form clusters at the corners and walls of the chamber. Triton X-100 is a nonionic surfactant with a hydrophilic chain and a hydrophobic group, and thus particles in the presence of Triton do not cluster but they stay suspended in the fluid.

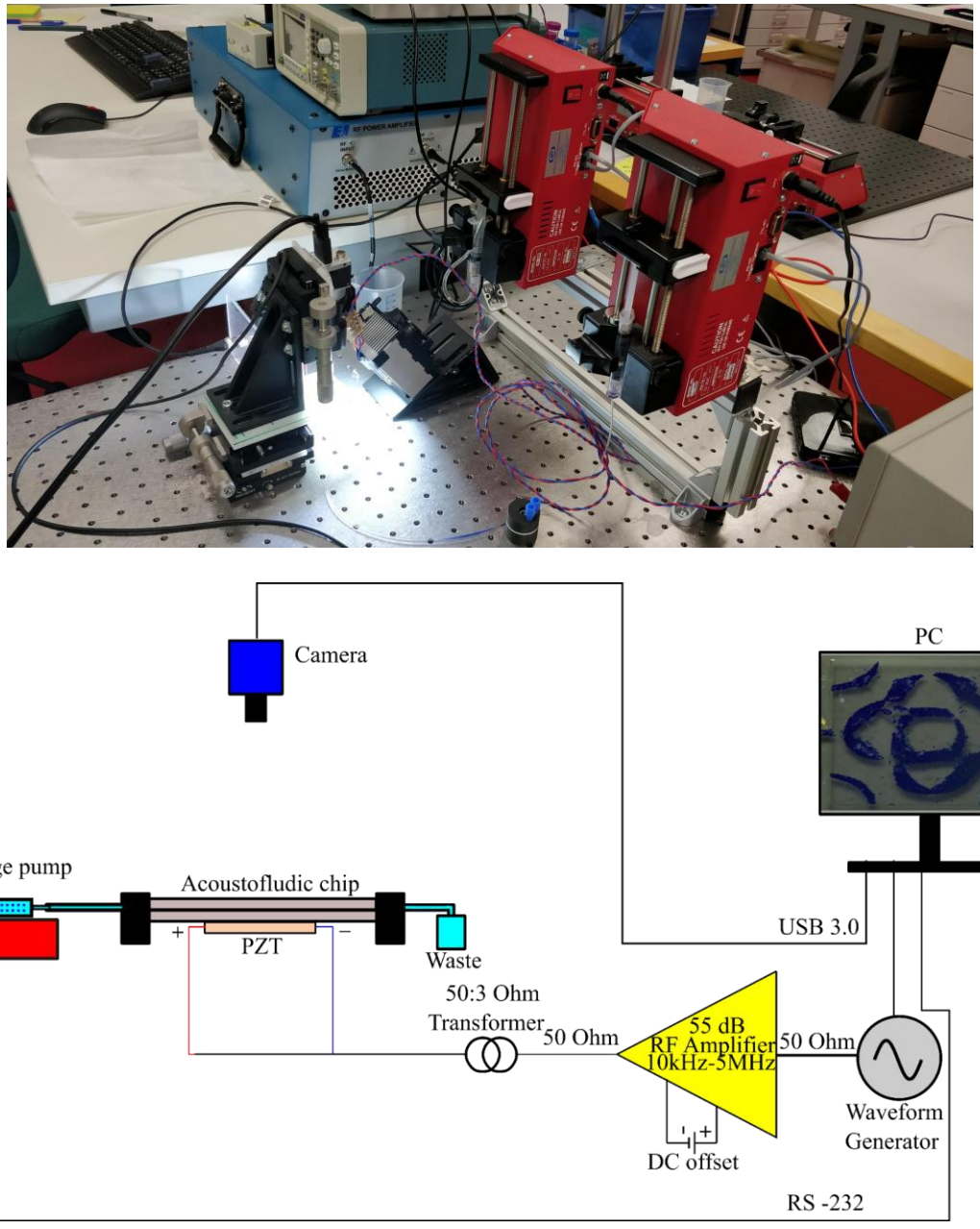

Figure 4.11. Actual and diagram representation of the experimental setup.

Figure 4.11 presents the experimental setup used to carry out the acoustofluidic experiments. Initially, the syringe pump was set to infuse at a flow rate of 9µl/min, to avoid bubble formation due to large pressures at the inlet. The syringe pump was stopped as soon as the acoustofluidic chamber was filled with the particle solution. Secondly, a signal was generated by a waveform generator (National Instruments PCI-5421), controlled using MATLAB®. The generated signal had a duration of 0.5 seconds, where 10 images were captured by using a machine vision camera while the chamber was actuating at different frequencies. The captured images were analyzed by a PTV script in MATLAB®, where the total particle movement was tracked for a) frequency scanning experiment, b) amplitude scanning experiment, and c) for reconstructing the acoustic patterns (Appendix A).

5. Results

5.1 Acoustic Simulations of Hard Wall and Full Chip Model

The results from the eigen frequency studies of all the acoustofluidic devices, were achieved by simulations as discussed in section 4.5. As mentioned in section 4.5, the fluidic walls of the chamber were modeled as sound hard wall boundaries for both PMMA, and glass. The natural frequencies then were acquired from the eigen frequency study, were it was found to have strong agreement with analytical frequency values found by solving eq. (6). The simulated and analytical values are presented in Appendix A. Continuing the simulations, the eigen frequency study of the full acoustofluidic device took place, where the boundary conditions were different on the chip interfaces:

1) Chip-air interface: sound soft boundary condition
2) Inlet-outlet: sound soft boundary condition.
3) Fluid- enclosing material interface: pressure continuity.

The results of this eigen frequency study presented an enormous difference between frequency values of the simulations assuming sound hard walls, and the full chip simulations specifically in the glass chip case. The differences in the eigen frequency values of the two models was attempted to be justified by modeling the full chip with variable densities of the glass. The aimed densities were increasing the acoustic impedance of glass by 10, 100, and 1000 times the original impedance value. As the density values of the glass increases, the more the frequencies and the eigen modes were approaching the ideal sound hard walls results of the chamber. These results are presented in Figure 5.1-2. The assumption of sound hard boundaries for internal walls of the glass chamber, is proven from these simulations that is not completely correct. This implies that only an artificial material with acoustic impedance as the $10\times$denser glass can consequently have an acoustic impedance of $10 \times Z_{\text{glass}}$,which can safely be modelled using sound hard wall boundaries.

5.2 Full Chip Simulations with Varying Materials

The results from the previous section 5.1, encouraged the study of eigenfrequencies in different materials, specifically materials that range from high, moderate, and low acoustic impedance. The simulations were carried out similarly with the glass full chip simulations mentioned previously. The values of density, and speed of sound used in this set of simulations can be found in references[42,44]. The first ten eigenfrequencies resulted from this set of simulations are presented in Figure 5.3, whereas the resulted six eigenmodes are presented in Figure 5.4 for platinum, mild steel, PMMA and PDMS. This set of results shows that material properties are dramatically affecting the resonance

frequency of a $\frac{n \cdot \lambda}{2}$ standing wave in a chamber. This can be observed from the following cases where platinum, and mild steel

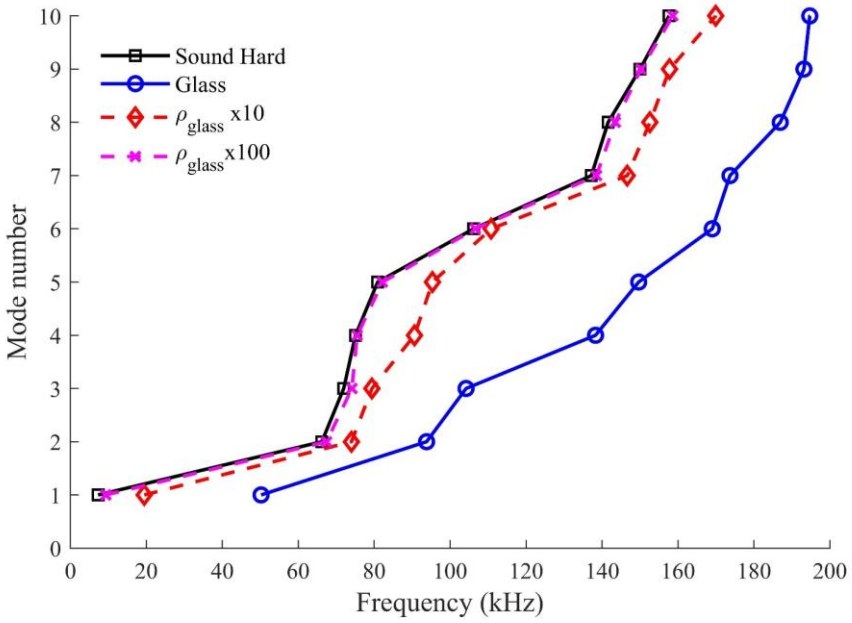

Figure5.1. Eigenfrequencies of a) hard wall chamber, b) ordinary glass, c) 10 times denser glass, d)100 times denser glass.

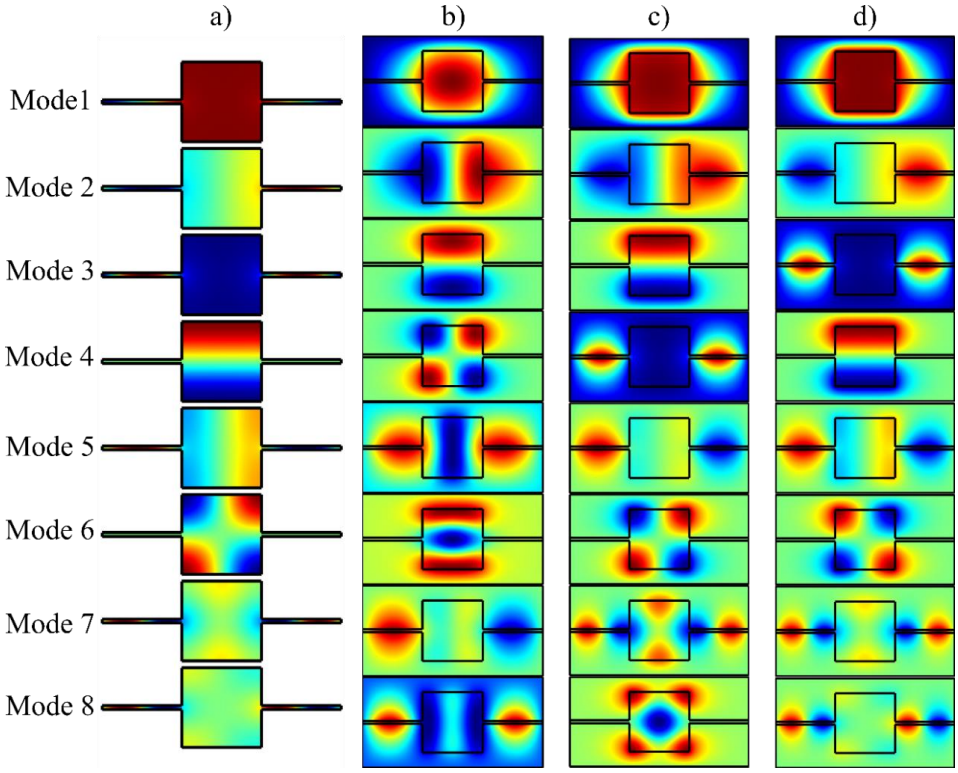

Figure 5.2. Eigenmodes of the glass chip for, a) hard wall chamber, b) normal glass, c) 10 times denser glass, d)100 times denser glass.

were both having high acoustic impedance, $Z \cong 70$ MRayls , $Z \cong 46$ MRayls.The eigenfrequencies of these two materials were found to be close to the ideal sound hard case in section 5.1, (Figure 5.1).

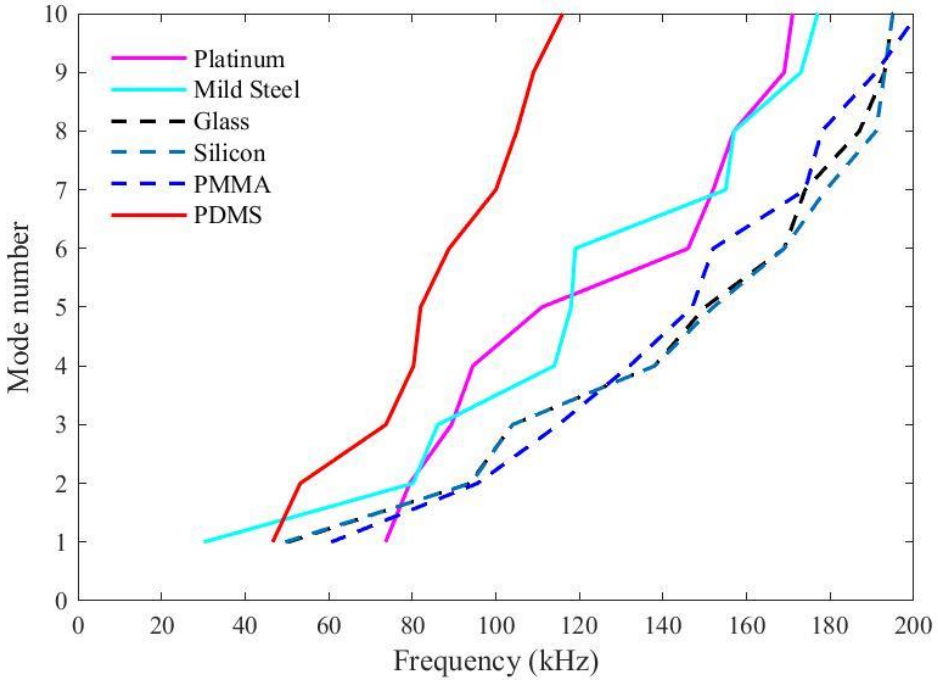

Figure 5.3. Eigen frequency study of different materials with high, medium and low acoustic impedance.

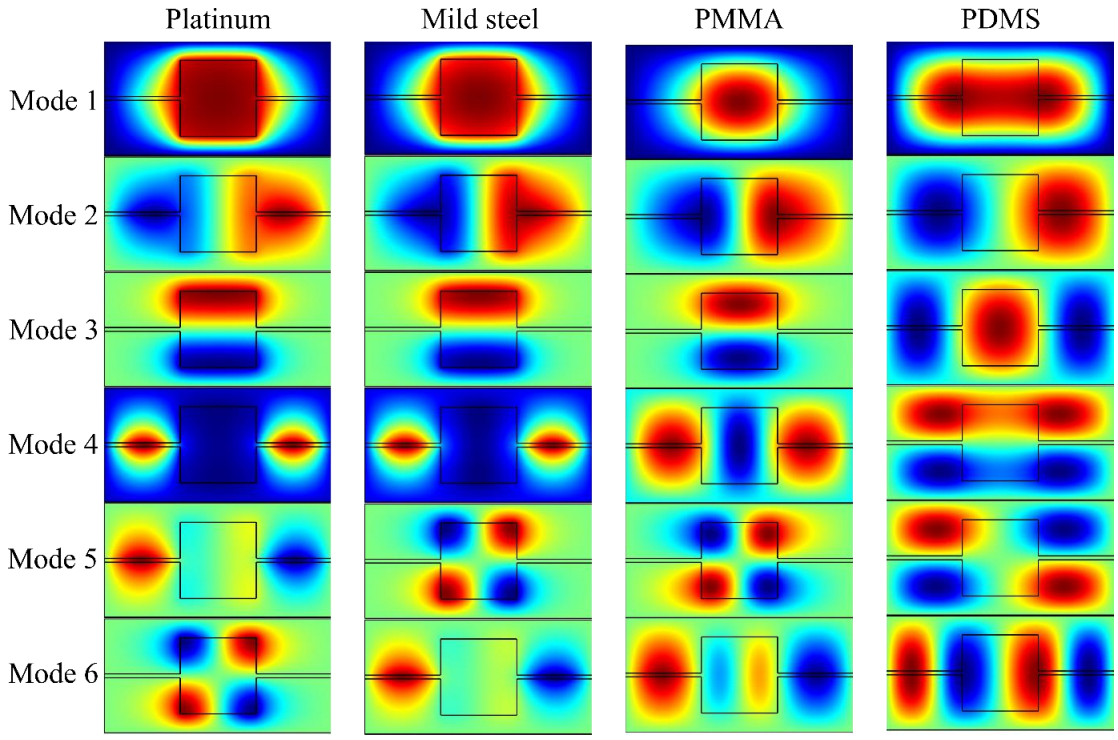

Figure 5.4. Eigenmodes of the materials with high, moderate and low acoustic impedance.

In contrast to the hard materials discussed earlier, PDMS was found to have a very low resonance frequency profile. However, the eigenmode patterns in the PDMS chip were comparable with acoustic modes found in other materials such as PMMA. Moreover, due to its very low acoustic impedance (poor acoustic properties), the standing waves in the PDMS full chip were formed at the edges of the chip instead at the edges of the microfluidic chamber, and thus its eigen frequencies are very low. For instance, the eighth eigenmode presented in PDMS is found at ~110 kHz, where in PMMA and glass their eighth eigenmodes are presented at ~190 kHz and, ~180 kHz, which is clearly an enormous difference in terms of frequency. Further, it was observed that the eigenfrequencies of silicon and glass are almost identical, despite the fact that their acoustic impedance differs by ~6 MRayls. By recalling the results from the previous section, we can say that neither glass or silicon is hard. At last, the PMMA chip found to have comparable eigenfrequencies with glass and silicon, where a minor frequency difference was presented at some eigenmodes.

The results of this study conclude that hard materials such mild steel, platinum and other metals are best suited for BAW acoustofluidics, due to their high acoustic impedances compared to PDMS and other softer materials. However, these materials despite their excellent acoustic characteristics, they lack microfabrication methods for e.g. fluidic channels, and are very rare in this field. On the other hand, materials such as PDMS showed that its eigenmodes do not occur within the chamber, but from the whole chip, and acts as a bulk resonator, which is not suitable for the nature this study. Additionally, the eigen frequency results of the acoustofluidic chips simulated by using glass, silicon, and PMMA materials were comparable. These results are leading into the assumption that these acoustofluidic chips in practice should have similar performance and similar eigenmode shapes.

5.3 Comparison of Eigen frequency and Frequency Domain Results

This section of results introduces the acoustic frequency response of the undamped PMMA, undamped PDMS, and glass full chip models. These simulations were done as described in section 4.5, where an acoustic monopole source was used to mimic the sound radiation of an actuating piezoelectric transducer. The resonance frequencies within the chamber were captured by a domain probe, where the captured quantities were frequency and absolute pressure. The frequency response of the three materials is presented in Figure 5.5. The resonance frequencies of the materials are presenting only the resonances of the acoustic chamber and excludes the resonances of the bulk device. The eigenfrequencies of the materials are presented in the same figure as their frequency response for comparison purposes.

Initially, the frequency response of the undamped PMMA chip shows that its first resonance appears at 60 kHz, which is identical to what we found by the eigen frequency study. However, the second and third acoustic modes of this chip were found in 132 kHz, and 173 kHz, whereas the second and third acoustic modes in the eigen frequency study were found at much lower frequency. The same was observed in the results obtained from the glass chip, where the first resonance frequency in both

cases have strong agreement. However, for the rest of the resonance frequencies of the frequency domain study, only every third eigen frequency was agreeing.

The reason lies on the symmetrical shape of the chamber and its uniform excitation by the monopole source. The symmetrical shape and excitation lead to the excitation of all symmetrical modes, where the probability to excite asymmetrical modes was eliminated.

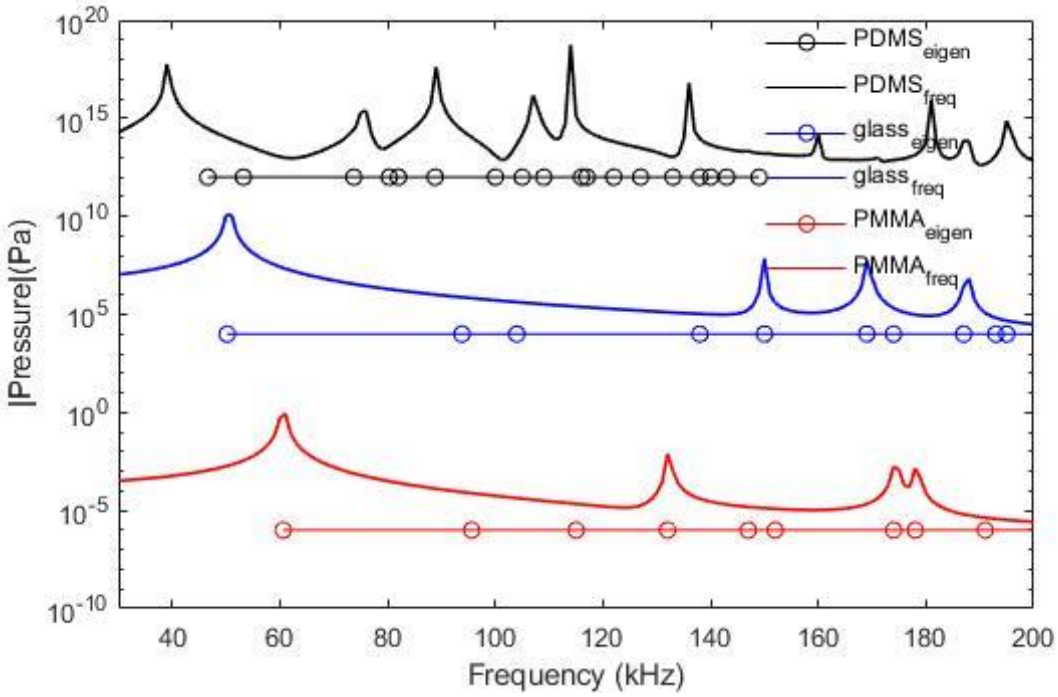

Figure 5.5. Simulated frequency response of Glass, PMMA, and PDMS.

In the Figure 5.5 above, we can see that the undamped PDMS has a very dense number of resonances in the same spectrum. The eigen frequency values of the PDMS chip do not clearly agree with the frequency domain results, despite their similar behavior. From the other hand, glass and the undamped PMMA full chip models behave in a similar manner, where their resonance frequencies are comparable (in the same range), and the number of resonance frequencies is the same. The close resonance relation of PMMA and glass chips was observed from the results acquired in the previous study. From this observation we can say that the frequency domain study in a sense confirms what we found previously in section 5.2. Since the frequency response of the undamped PMMA is comparable to the frequency response of glass chip, we can expect that the undamped PMMA chip in reality to perform similarly to a glass chip in acoustic micromanipulation applications. In order to validate more the results from both eigen frequency and frequency domain studies, a resonance frequency of the glass chip was selected (second harmonic) along with the corresponding acoustic pattern. In the same way, three eigen modes found in nearby eigen frequencies from the eigen frequency study of glass were acquired and compared with the aforementioned acoustic mode. The second harmonic of the glass chamber was found at 150 kHz, whereas the three nearest eigenmodes are found at 138 kHz,149.7 kHz and 169 kHz. The acoustic mode found in 150 kHz is identical with the eigenmode of 149.7 kHz,

which shows that these two studies have good agreement. However, in the eigen frequency study for a symmetric geometry, dual eigen modes are often observed (eigenmodes that share the same frequency). This cannot be observed in frequency domain with a symmetric source of excitation, because the modes will appear to be a by-product of two nearby eigen modes.

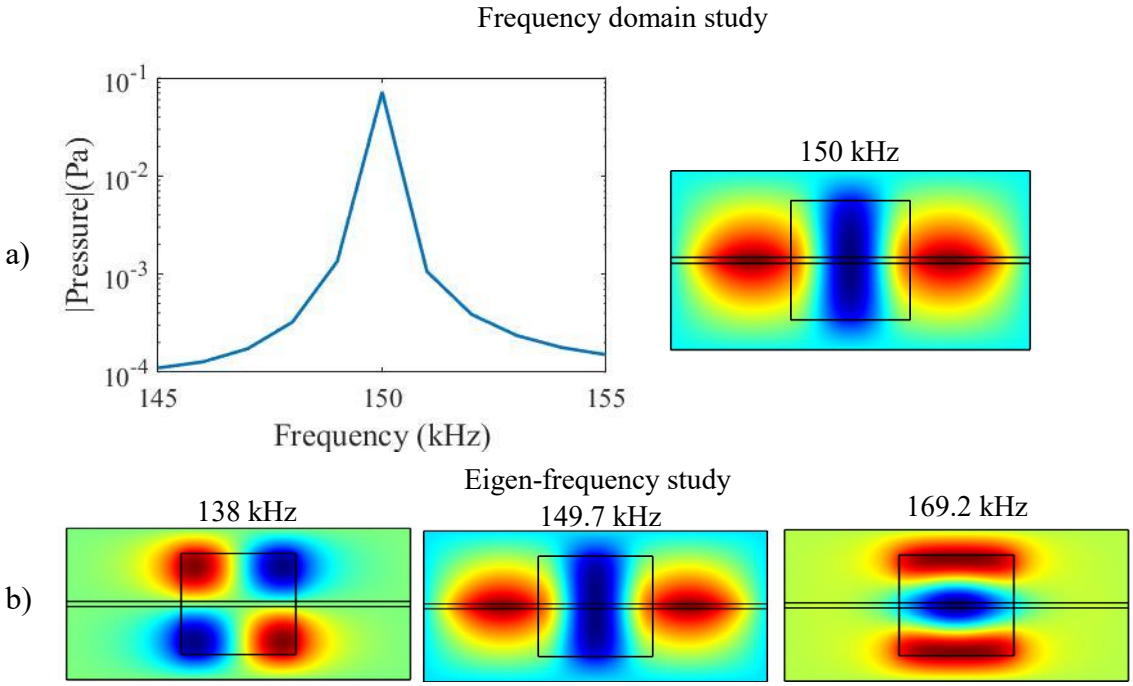

Figure 5.6. a) Acoustic resonance frequency, mode of glass chip at 150 kHz, found from frequency domain study, **b)** eigenmodes and eigenfrequencies of full chip glass model.

The results of the frequency domain study have strong agreement with eigen frequency study of all materials. The simulations using the frequency domain study for an acoustofluidic chip, should be carried out with caution, since real devices are not necessarily perfectly symmetric. In the case of a symmetric chip, the simulated modes might differ from the actual modes. Some of the following reasons can be the cause of that such as, misalignment of the actuator with the chamber, partially glued actuator, or high number of air-bubbles in the adhesive layer between chip and actuator, which will lead to poor wave propagation.

Additionally, in the results of eigen frequency study there are several eigen modes with a common frequency or nearby frequency (0.5-1 kHz difference in frequency). However, in the frequency domain study this is not possible, where mode duality can be detected only from the acquired patterns. In addition, combinations of two eigenmodes are often observed, which is a result of mode-mixing. These mixed modes cannot be found experimentally in a repeatable experiment, because for certain conditions the eigenmode A will present, while in a second repetition eigenmode B or a by-product of A and B might present. For this case the experimental validation of all existing eigen modes in the acoustofluidic chips will be hard or almost impossible.

5.4 Effect of Damping in PDMS-PMMA Simulations

Previously the frequency response of PMMA and PDMS chips took place, where these materials have been considered undamped and their lossy properties were ignored. In this part we will like to see the effects of damping on these materials. Does the attenuation coefficient affect only the pressure amplitude of the materials? Or it affects the resonance frequency also? The attenuation coefficients of both PMMA and PDMS were used in the damped device simulation by using the following values; $a_{\mathrm{PMMA}} \cong 0.4$ dB,and $a_{\mathrm{PDMS}} \cong 0.25$ dB per wavelength.[48]

The existence of damping in the case of PMMA shows that the resonance frequencies do not suffer any frequency shifts, however at 173-179kHz the double resonance frequency suffers of merging. On the other hand, the fundamental resonance of PMMA overshoots in amplitude, whereas the resonances above the fundamental frequency drop dramatically as the frequency increases.

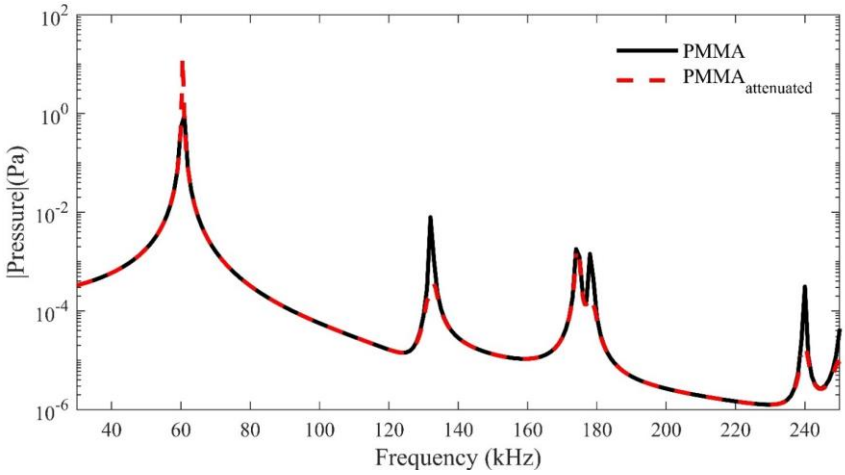

Figure 5.7. Frequency responses of the undamped and damped PMMA chip.

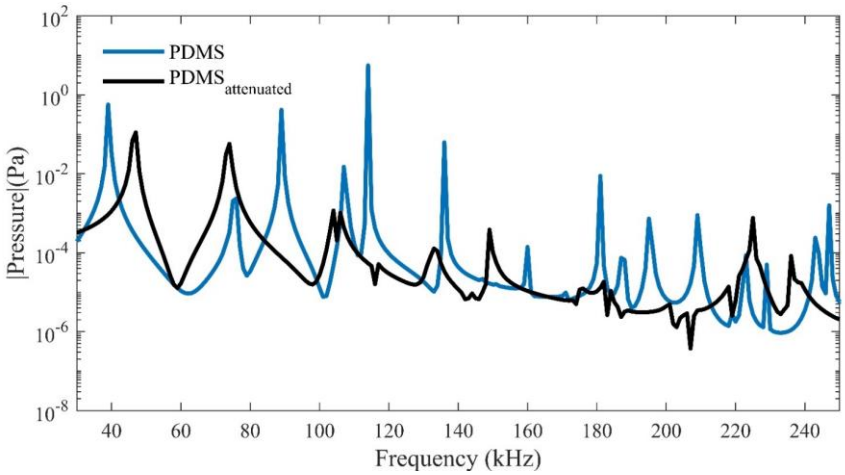

Figure 5.8. Frequency responses of the undamped and damped PDMS chips.

In the damped PDMS case, the first resonance (Figure 5.8), experiences a frequency shift of 10 kHz towards the right side of the graph, while the rest of the resonances are shifted towards the left. In addition, the frequency shifts of the resonances do not have a constant frequency shift value, and the number of resonances has declined significantly. The pressure amplitudes of the damped PDMS chip were attenuated far more than in the PMMA case. It can be seen by Figure 5.8 that the pressure amplitude decreases enormously, and several low amplitude resonance were 'filtered out'. Generally, the presence of damping in the enclosing material will affect the overall behavior of the standing waves due to changes in the frequency behavior of the device, and the heavy pressure losses such in the PDMS case. This can happen when the attenuation coefficient is relatively high, which mainly affects both the amplitude of the resonance frequencies along with the actual resonance frequency. The importance of adding the damping coefficient in simulations, prior to the actual fabrication of an acoustofluidic device made out of plastic is significant, because their behavior changes dramatically.

For a harder plastic such as PMMA, we can see that the component getting affected by the attenuation coefficient is the pressure amplitude, which might be the case even for other hard engineering plastics. If the previous speculation is true, then hard plastics can have a future in the field of acoustofluidics, because of their ease fabrication methods, and predictable frequency response.

5.5 Comparison of Experimental Chladni Patterns and Simulations

In this section, experimental acoustic modes will be shown, and they will be compared with results obtained by the previous eigen frequency and frequency domain study. The following Figure 5.9 presents ten acoustic modes captured throughout the experiment in the glass chip.

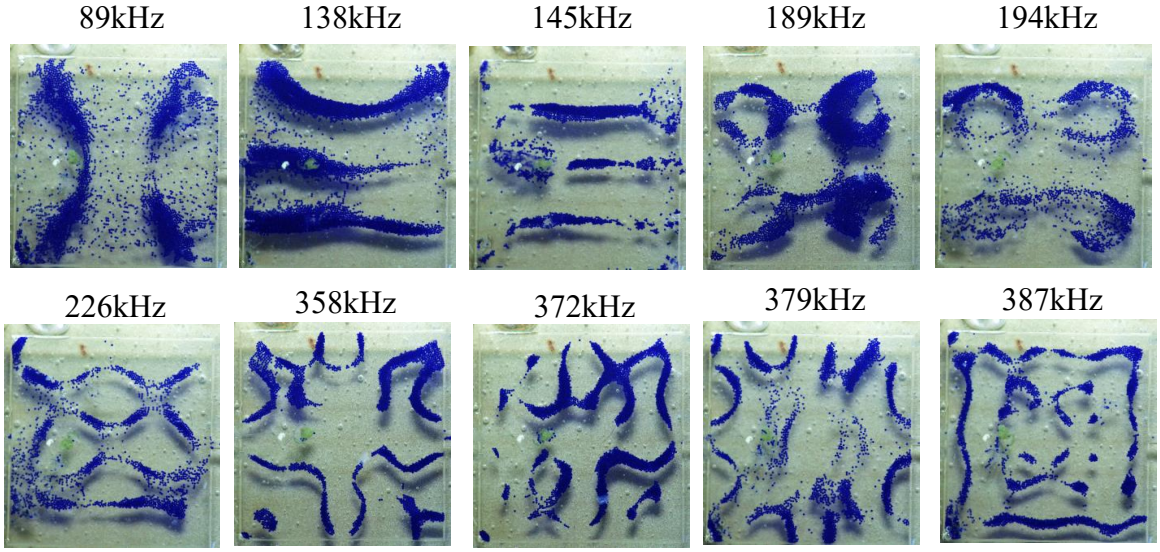

Figure 5.9. Experimental acoustic modes in glass acoustofluidic chip, visualized by 100 µm blue polystyrene particles.

Additionally, in Figure 5.10, an acoustic pattern is selected to be compared with the same eigenmode acquired from the eigen frequency study, and three acoustic modes at the same frequency range from frequency domain study. Equivalent acoustic modes of PMMA are not yet available, however, some preliminary patterns obtained by ongoing experiments of the PMMA chip are presented in Appendix A along with their PTV.

The experimental acoustic modes of the glass do not correlate with acoustic modes found in the simulation studies in this thesis. However, from the eigen frequency study some of the modes were identified, whose frequency was higher by 75 -100 kHz than the actual modes. The actual acoustic mode of the Figure 5.10 represents three nodal lines, which in the ideal case this mode is $n_x = 0, n_y = 3$. The frequency for this mode can be found by a simple substitution of the speed of sound in water ($1500\ \mathrm{ms}^{-1}$), and by including the lateral dimensions of the chamber in eq. (6). The resonance frequency for $n_x = 0, n_y = 3$ was found at 225 kHz. Similar frequency value was acquired from the eigen frequency study for the same eigenmode. The eigen frequency was found at 239 kHz and it is presented in Figure 5.10.

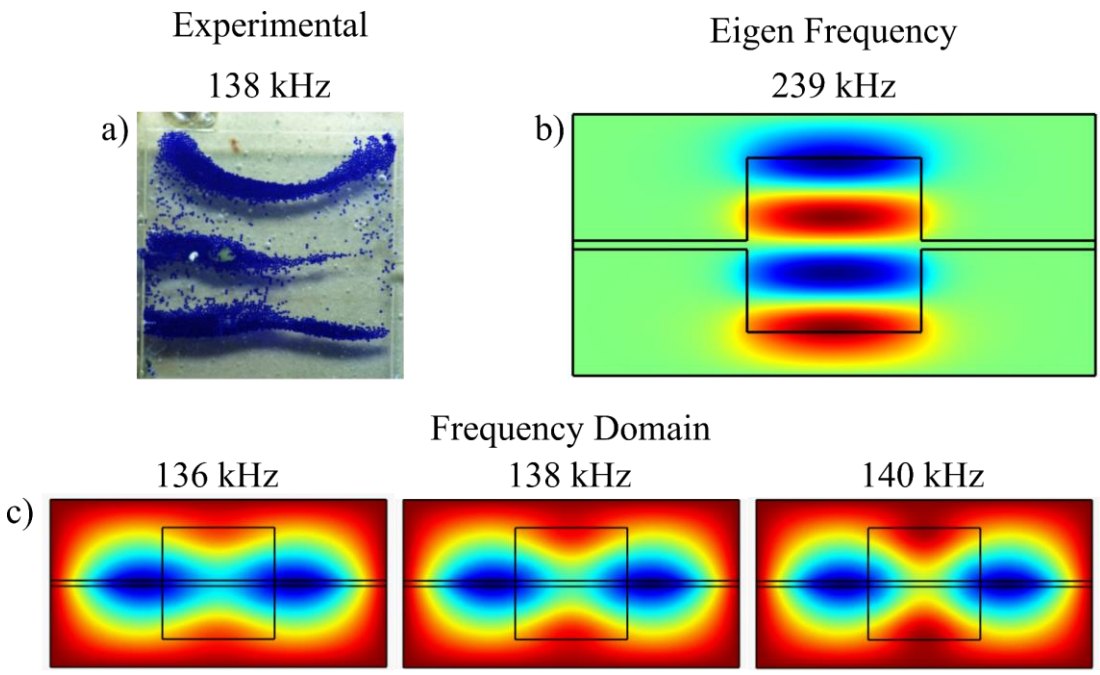

Figure5.10. a) Experimental acoustic mode at 138 kHz, **b)** Equivalent eigen mode by eigen frequency study, and **c)** frequency domain acoustic modes.

The simulations so far do not agree with the results acquired from the experiments. However, the acoustic modes of the experiments have their frequency 75-100 kHz lower from what we observed by the eigen frequency study. Additionally, by using the eq. (6) and the speed of sound of water the resulted frequency agrees with the eigen frequency of the same mode. However, this implies that the speed of sound of the fluid used in the chip has different speed of sound that what it was assumed to be. By rearranging eq. (6) for the actual frequency of the acoustic mode 138 kHz, the speed of sound

was found to be $920\ \mathrm{ms}^{-1}$, which is very low and cannot be true for water, which leads to the case of a possibly misplaced or partially delaminated actuator. In order to justify this enormous frequency difference of the experimental − theoretical modes and frequencies, re-coupling of the piezoelectric transducer and the device should be performed.

5.6 Mixing Efficiency

Mixing of the polystyrene microparticles was achieved by the methods described earlier in this thesis work (section 4.4). In the experimental processes, mixing of the microparticles was found to be beneficial for the better imaging of the acoustic modes, and for the particles tracking algorithm. Redistribution of microparticles within the chamber was performed at every frequency, for better Chladni pattern formation. This is in a sense it is similar to what Ernst Chladni was doing in his experiments, for every excitation frequency of the plates, he was adding sand grains to achieve uniform distribution over the plates. In order to quantify the efficiency of the mixing processes in the PMMA and glass chip, Chi-squared method was employed. The results of this statistical approach showed that the particle distribution within the glass chamber is not random, and thus not uniform. However, this is not that obvious from the recorded images and from the heatmaps in c), and d) in the Figure 5.9 below. The P value resulted by applying the Chi-squared method in the mixing process of glass chamber was $\mathrm{P} = 2.80^{-13}$.

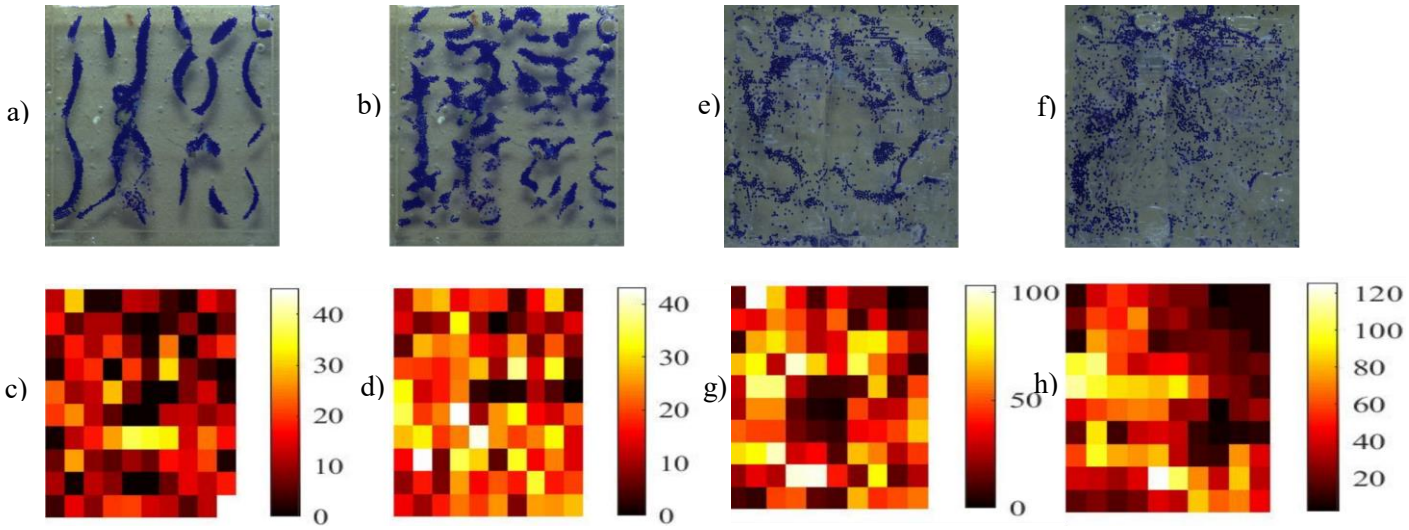

Figure 5.9. a) Particles before mixing in glass, **b)** heatmap plot of initial particle distribution, **c)** Particles after mixing, **d)** heatmap plot of mixed particles. **e)** Particles before mixing in PMMA, **f)** heatmap plot of initial particle distribution, **g)** Particles after mixing, **h)** heatmap plot of mixed particles.

Similarly, the mixing efficiency of the PMMA chip was also calculated by Chi-squared method. The resulted P value was found to be $\mathrm{P} = 2.18^{-10}$, which shows that the particle distribution in the fluidic chamber is also not random. However, by comparing a)-d) to e)-h) in Figure 5.9, we can say that

acoustic streaming in PMMA achieves better particle distribution than particle alignment method used in glass.

Even though the mixing processes were not statistically proven to be very effective, their existence is very essential in the following experiments. Firstly, in PTV mixing was found to enhancing the area covered by particles, which helps PTV to capture more information from particles under the effects of standing waves. Secondly in amplitude and frequency scanning experiments, mixing re-establishes particle uniformity within the chamber, so that PTV can accurately capture particle mobility. Lastly, particle mixing enhances the results of the acoustic pattern formation experiment, since it distributes the particle in the chamber while breaking previous made clustered patterns.

5.7 Preliminary Results of Particle Tracking Velocimetry

Particle tracking velocimetry of the polystyrene microparticles is still work on progress, where the main goal is to monitor and track the motion of individual microparticles. In this preliminary state of PTV, the results are often suffering from particle clusters in the chamber, which makes it impossible for PTV to identify all the particles in this case. PTV is one of the basic applications of the proposed mixing of microparticles within the chamber, to enrich particle imaging. In this current state we can show how our PTV algorithm performs and what is the current outcome. The following Figure 5.11 shows a) the acoustic mode obtained from the experiment, whereas b) and c) show the heatmap magnitude of particle mobility captured from PTV, and quiver plot of the actual particle movement in the chamber.

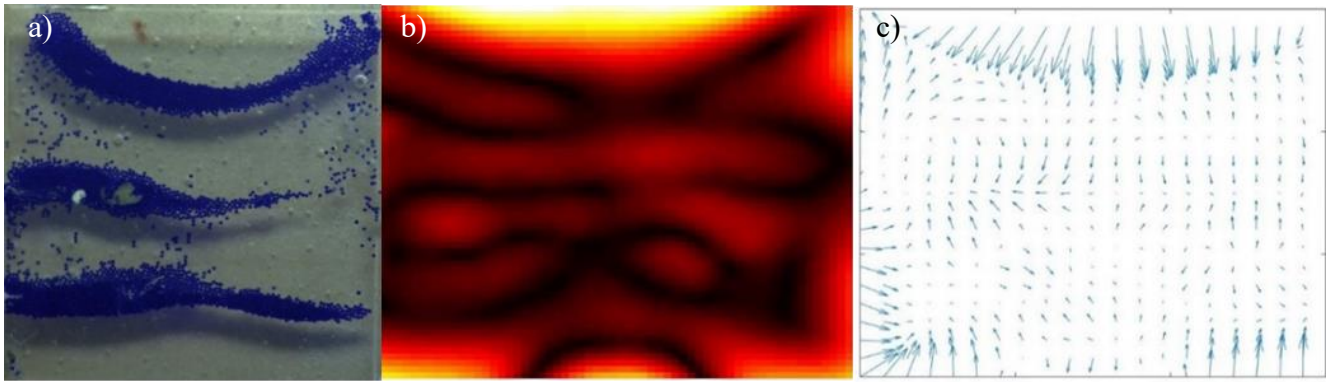

Figure 5.11. a) Acoustic pattern obtained at frequency 138 kHz, **b)** heatmap of the magnitude of particle mobility captured via PTV (black color denotes pressure nodes and red-yellow color denotes pressure antinodes), and **c)** quiver plot of PTV data.

The heatmap plot of the data captured by PTV do not replicate the Chladni pattern very accurately, which is why more PTV results were not shown in this thesis work. Further work needs to be done in order to enhanced particle readability by the machine vision system, which will significantly improve the performance of the PTV algorithm, and future particle tracking in control manipulations of particles.

6. Conclusions

In thesis the preliminary study of different materials for particle micromanipulation applications was done. The results from this thesis work shows that the PDMS is not suitable for these applications, due to its poor acoustic properties, and large attenuation coefficient. Additionally, in both eigen frequency and frequency domain studies standing waves in PDMS were formed from the edges of the chip instead from the edges of the chamber. However, the results of these studies for PMMA showed that this material can perhaps be used for acoustically micro manipulating particles by BAW. Additionally, in the case of the undamped PMMA chip, the resonance frequencies of the chip were found to be comparable with the resonance frequencies of glass chip. These results are still comparable with the glass chip even when the attenuation coefficient was added in the PMMA chip. Since the presence of attenuation in the material did not added significant frequency shifts at resonances but attenuated heavily at higher resonance frequencies. In the case of the glass chip, was found that the assumption of hard walls on the fluid-glass chamber interface does not really stand. This was found in the eigen frequency study of glass chip, where the results from both studies hard wall assumption and full modelled glass chip are unrelated. In addition, the glass as fluid enclosing material can be assumed as sound hard material only if artificially its density increases by 10 or 100 times its original value (Figure 5.1). It is clear that using FEM packages such as COMSOL, it is a powerful and fast way to understand and evaluate a particular design for complicated physics and structures. Simulations with such software has gained us a better understanding in how different materials behave with ultrasound, and how the sound excitation location can affect the acoustic patterns and resonance frequencies of the chamber. However, the results acquired by the actual experiments do not match any of the simulated results at the same frequencies. Moreover, the actual acoustic modes were observed at frequencies 75-100kHz below the frequencies found in theory.

6.1 Future Work:

As further work beyond this thesis work, additional simulations of different boundary conditions, and excitation areas- sources are needed for the current acoustofluidic chambers. These different simulations should be executed carefully, since different boundaries, and different excitation areas can cause a significant change of the acoustic modes. This change can lead the theoretical modes to match the experimental modes.

From experimental point of view more materials should be explored, if the costs of buying and fabrication methods allow us to do so. As in the case of platinum and mild steel, which both have very high acoustic impedance. Some possible method of microfabricating microchannels in such materials can be direct milling over their surface. If this is possible then these devices would be more preferable than glass or PMMA, due to their excellent performance in simulations. However, the usage of steel and platinum are not very common in microfluidics, which can lead into a rapid increase of costs, while the acoustic performance in acoustofluidic applications was not reported in literature.

References

1. Chin, C. D. *et al.* Microfluidics-based diagnostics of infectious diseases in the developing world. *Nat. Med.* **17,** 1015–1019 (2011).

2. Huang, H.-Y., Lai, Y.-L. & Yao, D.-J. Dielectrophoretic Microfluidic Device for in Vitro Fertilization. *Micromachines* **9,** 135 (2018).

3. He, J. H. *et al.* Biomicrofluidic lab-on-chip device for cancer cell detection. *Appl. Phys. Lett.* **93,** 223905 (2008).

4. Dubin, C. H., Bermingham, J. A., Josef Bossart & Symank, K. DRUG DEVICE MARKET MARKET MARKET DIABETES TESTING MARKET ALBUMIN MARKET Tapered Needle Technology. in **15,** (2015).

5. Yager, P. *et al.* Microfluidic diagnostic technologies for global public health. *Nature* **442,** 412–418 (2006).

6. Vinet, L. & Zhedanov, A. A 'missing' family of classical orthogonal polynomials. *J. Phys. A Math. Theor.* **44,** 085201 (2011).

7. Huang, X., Zhang, Y., Liu, Y. & Hu, Z. Effect of small amount of nitrogen on carbide characteristics in unidirectional Ni-base superalloy. *Metallurgical and Materials Transactions A: Physical Metallurgy and Materials Science* **28,** 2143–2147 (1997).

8. Ashraf, M. W., Tayyaba, S. & Afzulpurkar, N. Micro Electromechanical Systems (MEMS) Based Microfluidic Devices for Biomedical Applications. 3648–3704 (2011). doi:10.3390/ijms12063648

9. Pethig, R. *Dielectrophoresis*. *Dielectrophoresis* **i,** (John Wiley & Sons, Ltd, 2017).

10. Jo, Y., Hahn, Y. K. & Park, J. K. A magnetophoresis-based microfluidic detection platform under a static-fluid environment. *Microfluid. Nanofluidics* **21,** (2017).

11. Khriplovich, I. B. & Pomeransky, A. A. Equations of Motion of Spinning Relativistic Particle in Electromagnetic and Gravitational Fields. *Uma ética para quantos?* 81–87 (1998). doi:10.1080/01422419908228843

12. Yan, Y., Guo, D. & Wen, S. Joule Heating Effects on Two-phase Flows in Dielectrophoresis Microchips. **11,** 196–205 (2017).

13. Yang, L., Banada, P. P., Bhunia, A. K. & Bashir, R. Immuno-reactivity of Listeria monocytogenes. **14,** 1–14 (2008).

14. Chladny, E. F. F. *Entdeckungen über die Theorie des Klanges*. (1787).

15. Spengler, J. F., Coakley, W. T. & Christensen, K. T. Microstreaming effects on particle concentration in an ultrasonic standing wave. *AIChE J.* **49,** 2773–2782 (2003).

16. Bengtsson, M. & Laurell, T. Ultrasonic agitation in microchannels. *Anal. Bioanal. Chem.* **378,** 1716–1721 (2004).

17. Petersson, F., Nilsson, A., Holm, C., Jönsson, H. & Laurell, T. Separation of lipids from blood utilizing ultrasonic standing waves in microfluidic channels. *Analyst* **129,** 938–943 (2004).

18. Hagsäter, S. M., Jensen, T. G., Bruus, H. & Kutter, J. P. Acoustic resonances in microfluidic chips: full-image micro-PIV experiments and numerical simulations. *Lab Chip* **7,** 1336 (2007).

19. Leibacher, I., Reichert, P. & Dual, J. Microfluidic droplet handling by bulk acoustic wave (BAW) acoustophoresis. *Lab Chip* **15,** 2896–2905 (2015).

20. Fornell, A., Ohlin, M., Garofalo, F., Nilsson, J. & Tenje, M. An intra-droplet particle switch for droplet microfluidics using bulk acoustic waves. *Biomicrofluidics* **11,** 031101 (2017).

21. Lenshof, A., Evander, M., Laurell, T. & Nilsson, J. Acoustofluidics 5: Building microfluidic acoustic resonators. *Lab Chip* **12,** 684 (2012).

22. Savage, W. J., Burns, J. R. & Fiering, J. Safety of acoustic separation in plastic devices for extracorporeal blood processing. *Transfusion* **57,** 1818–1826 (2017).

23. Silva, R. *et al.* Rapid prototyping and parametric optimization of plastic acoustofluidic devices for blood–bacteria separation. *Biomed. Microdevices* **19,** 70 (2017).

24. Bruus, H. Acoustofluidics 1: Governing equations in microfluidics. *Lab Chip* **11,** 3742 (2011).

25. Bruus, H. Acoustofluidics 2: perturbation theory and ultrasound resonance modes. *Lab Chip* **12,** 20–28 (2012).

26. Barnkob, R. Acoustofluidics in microsystems : investigation of resonances. *Master Thesis* 138 (2009).

27. Bruus, H. Acoustofluidics 1: Governing equations in microfluidics. *Lab Chip* **11,** 3742–51 (2011).

28. Devendran, C., Gralinski, I. & Neild, A. Separation of particles using acoustic streaming and radiation forces in an open microfluidic channel. *Microfluid. Nanofluidics* **17,** 879–890 (2014).

29. King, L. V. On the acoustic radiation pressure on spheres. *Proc. R. Soc. London. Ser. A. Math. Phys. Sci.* **147,** 212–240 (1934).

30. Yosioka, K. & Kawasima, Y. Acoustic radiation pressure on a compressible sphere. *Acustica* **5,** 167–173 (1955).

31. Gor'kov, L. P. Forces acting on a small particle in an acoustic field within an ideal fluid. *Dokl. Akad. Nauk SSSR* **140,** 88–91 (1961).

32. Lenshof, A., Magnusson, C. & Laurell, T. Acoustofluidics 8: applications of acoustophoresis in continuous flow microsystems. *Lab Chip* **12,** 1210–23 (2012).

33. Friend, J. & Yeo, L. Y. Microscale acoustofluidics: Microfluidics driven via acoustics and ultrasonics. *Rev. Mod. Phys.* **83,** 647–704 (2011).

34. Oberti, S. Micromanipulation of Small Particles within Micromachined Fluidic Systems. 160 (2009).

35. Wiklund, M., Green, R. & Ohlin, M. Acoustofluidics 14: Applications of acoustic streaming in microfluidic devices. *Lab Chip* **12,** 2438 (2012).

36. Bruus, H. Theoretical microfluidics. *Physics (College. Park. Md).* **18,** 363 (2008).

37. Bruus, H. Acoustofluidics 10: Scaling laws in acoustophoresis. *Lab Chip* **12,** 1578 (2012).

38. Muller, P. B., Barnkob, R., Jensen, M. J. H. & Bruus, H. A numerical study of microparticle acoustophoresis driven by acoustic radiation forces and streaming-induced drag forces. *Lab Chip* **12,** 4617 (2012).

39. Dorrestijn, M. *et al.* Chladni figures revisited based on nanomechanics. *Phys. Rev. Lett.* **98,** 026102 (2007).

40. Groschl, M. Ultrasonic Separation of Suspended Particles - Part I : Fundamentals. *acta Acust.* (1998). doi:10.1109/ULTSYM.2001.991812

41. Evander, M. & Nilsson, J. Acoustofluidics 20: Applications in acoustic trapping. *Lab Chip* **12,** 4667 (2012).

42. NDTnet. Plastic Material's acoustic properties. Available at: https://www.ndt.net/links/proper.htm. (Accessed: 10th March 2019)

43. Nama, N. *et al.* Numerical study of acoustophoretic motion of particles in a PDMS microchannel driven by surface acoustic waves. *Lab Chip* **15,** (2015).

44. Bloornfield, P. E. Experimental study of the acoustical properties of polymers utilized to construct PVDF ultrasonic transducers and the acousto-electric properties of PVDF and P(VDF/TrFE) films. *IEEE Trans. Ultrason. Ferroelectr. Freq. Control* **47,** 1397–1405 (2000).

45. Bamshad, A., Nikfarjam, A. & Khaleghi, H. A new simple and fast thermally-solvent assisted method to bond PMMA-PMMA in micro-fluidics devices. *J. Micromechanics Microengineering* **26,** (2016).

46. Al-Halhouli, A., Al-Faqheri, W., Alhamarneh, B., Hecht, L. & Dietzel, A. Spiral Microchannels with Trapezoidal Cross Section Fabricated by Femtosecond Laser Ablation in Glass for the Inertial Separation of Microparticles. *Micromachines* **9,** 171 (2018).

47. Lowson, M. V. Introduction to acoustics 1970. *J. Sound Vib.* **14,** 550 (1971).

48. Cafarelli, A. *et al.* Tuning acoustic and mechanical properties of materials for ultrasound phantoms and smart substrates for cell cultures. *Acta Biomater.* **49,** 368–378 (2017).

Appendix A: Frequency Responses of PMMA and Glass Chips

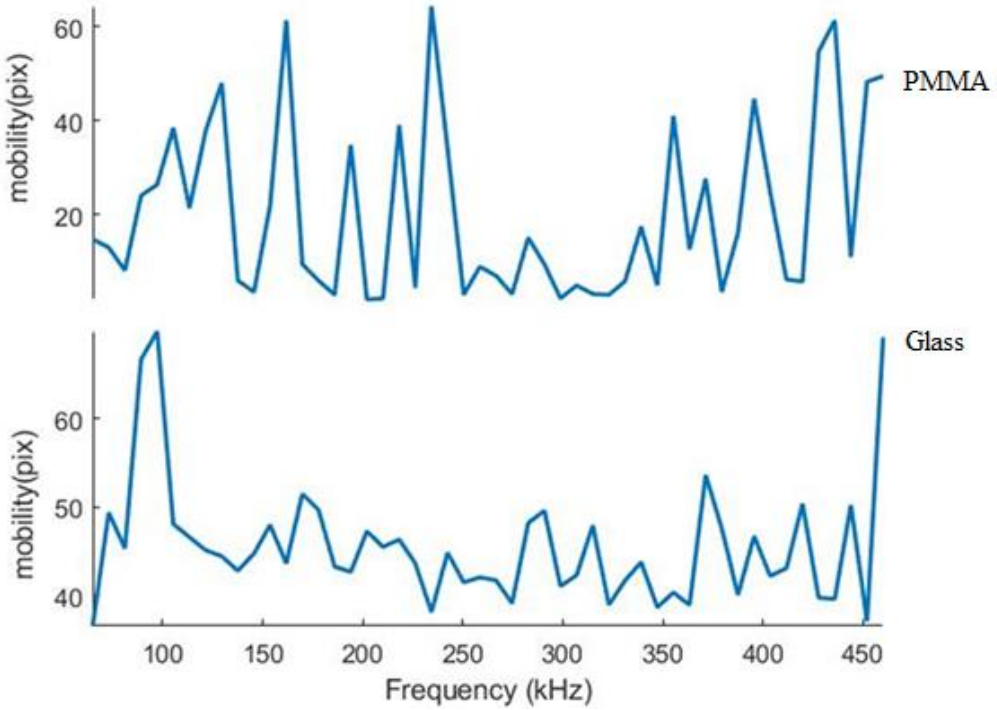

Figure A.1. Frequency responses of the PMMA and Glass acoustofluidic chips

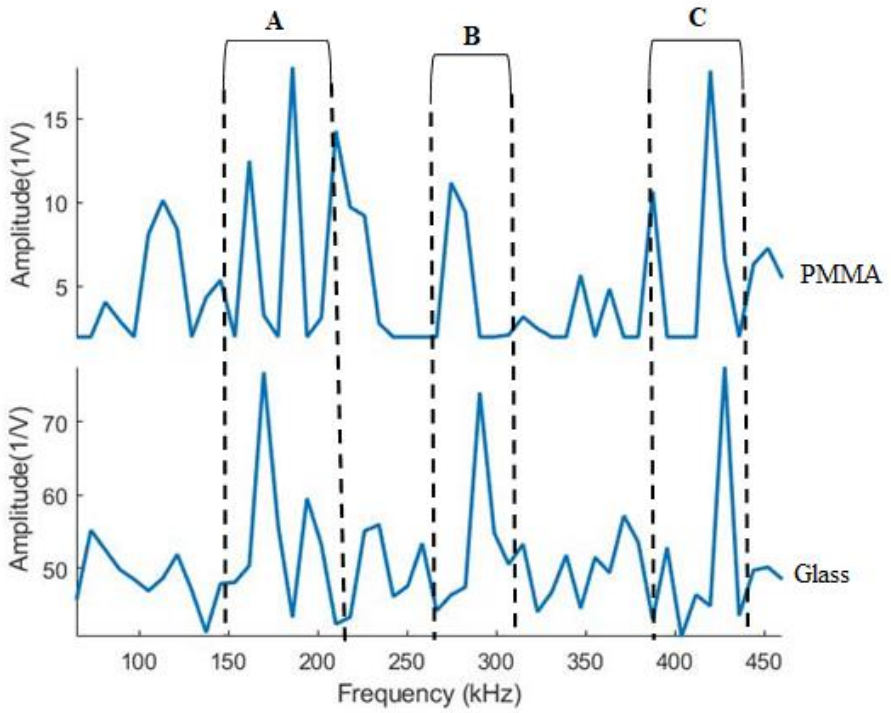

Figure A.2. Amplitude response of PMMA and Glass acoustofluidic chips

Table A.1. Analytical and Numerical frequencies of PMMA, PDMS and Glass chips

Mode number (nx,ny)	Analytical frequencies (kHz)	PDMS: Numerical Eigen frequency (kHz)	PMMA: Numerical Eigen frequency (kHz)	Glass: Numerical Eigen frequency (kHz)
nx=0,ny=1	75	-	74.650	74.650
nx=1,ny=0	75	-	74.71	74.71
nx=1,ny=1	106.07	105.5	105.66	105.66
nx=2,ny=1	167.705	166.67	163.17	163.17
nx=1,ny=2	167.705	166.69	166.98	166.98
nx=2,ny=2	212.132	211.14	213.17	213.17

Appendix B: Preliminary Particle Tracking Velocimetry of Glass and PMMA chips

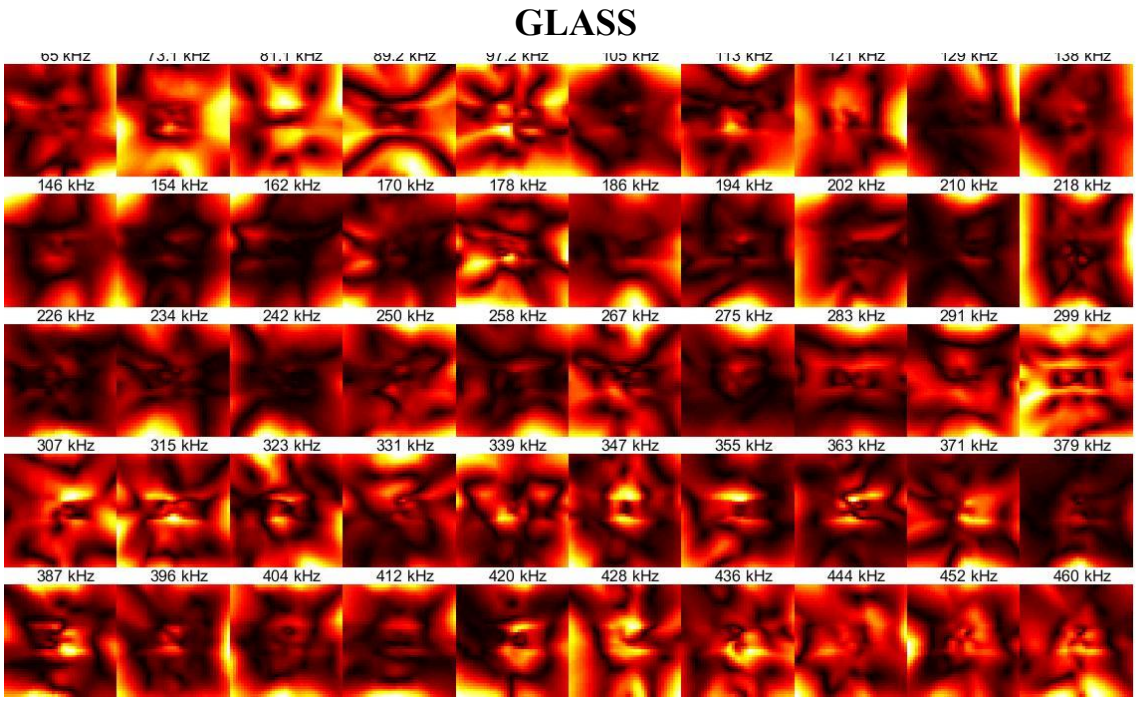

Figure B.1. Preliminary PTV heatmap plots of particle motion within glass chip for frequencies 65-460 kHz.

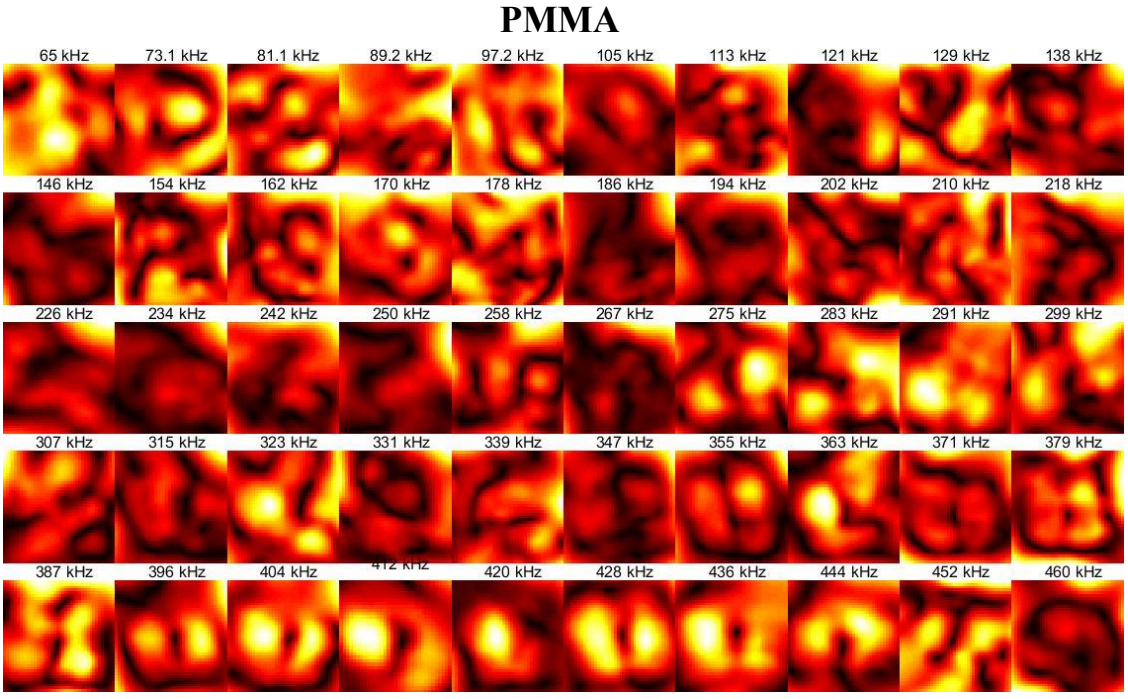

Figure B.2. Preliminary PTV heatmap plots of particle motion within PMMA chip for frequencies 65-460 kHz.